UNIVERSIDAD DE INVESTIGACIÓN DE TECNOLOGÍA EXPERIMENTAL YACHAY

Escuela de Ciencias Físicas y Nanotecnología

TÍTULO: The Study of Diatoms Doped with Nanoparticles for Atrazine Adsorption

Trabajo de integración curricular presentado como requisito para la obtención del título de Ingeniero en Nanotecnología

Autor:

Aguilar Ramirez Melany Nicole

Tutor:

PhD – Briceño Araujo Sarah Elisa

Co-tutor:

PhD – González Gema

Urcuquí, Diciembre, 2023

AUTORÍA

Yo, **AGUILAR RAMIREZ MELANY NICOLE**, con cédula de identidad 1726918616, declaro que las ideas, juicios, valoraciones, interpretaciones, consultas bibliográficas, definiciones y conceptualizaciones expuestas en el presente trabajo; así cómo, los procedimientos y herramientas utilizadas en la investigación, son de absoluta responsabilidad de el/la autora (a) del trabajo de integración curricular. Así mismo, me acojo a los reglamentos internos de la Universidad de Investigación de Tecnología Experimental Yachay.

Urcuquí, Diciembre, 2023.

Firmado electrónicamente por:
MELANY NICOLE
AGUILAR RAMIREZ

_____

Melany Nicole Aguilar Ramirez
CI: 1726918616

AUTORIZACIÓN DE PUBLICACIÓN

Yo, **AGUILAR RAMIREZ MELANY NICOLE,** con cédula de identidad 1726918616, cedo a la Universidad de Investigación de Tecnología Experimental Yachay, los derechos de publicación de la presente obra, sin que deba haber un reconocimiento económico por este concepto. Declaro además que el texto del presente trabajo de titulación no podrá ser cedido a ninguna empresa editorial para su publicación u otros fines, sin contar previamente con la autorización escrita de la Universidad.

Asimismo, autorizo a la Universidad que realice la digitalización y publicación de este trabajo de integración curricular en el repositorio virtual, de conformidad a lo dispuesto en el Art. 144 de la Ley Orgánica de Educación Superior

Urcuquí, Diciembre, 2023.

Firmado electrónicamente por:
MELANY NICOLE
AGUILAR RAMIREZ

_____

Melany Nicole Aguilar Ramirez
CI: 1726918616

Dedication

This first step into my professional project disposed is dedicated to the core of my life, the women who has never let me to give up at any time in any place. This is dedicated to my beloved mom, Cecilia Ramirez.

Melany Nicole Aguilar Ramirez

Acknowledgments

I would like to express my immense gratitude to my advisor Prof. Sarah Briceño for all the support since my beginnings in research. I am very grateful with her for her guidance in this process as well as her patience and motivation at every step. Her great knowledge shared towards me during this process both in the laboratory and when writing my degree project. I would also like to express my gratitude to my co-advisor Prof. Gema Gonzalez who, like Prof. Sarah Briceño, guided me in this process and supported my academic and professional growth with her vast experience in the field of research.

I would also like to thank my fellow classmates and friends from university who have been with me during different and challenging stages of my academic journey. In particular, I would like to express my gratitude to my roommate Karen Albán for her support from the very first day of university, during late-night study sessions, and moments of leisure. I also want to give special thanks to my two friends and colleagues, Daniela Serrano and Cristina Rubio, who have been of vital importance, support, and motivation in achieving my goals during the past year.

Last but certainly not least, I want to express my gratitude to my life's daily motivation, my family. Thanks to my mother, Cecilia, for being that life engine that inspires me every day, to my sister Isabela for being that unwavering support, and to my brother Thomas for always challenging me to do things better. Finally, I want to thank my partner, friend, colleague, and love, Alexis Garzón who has been by my side every step of this exhausting journey, always pushing me to be better, helping me up after every stumble, and teaching me about the beauty of life.

Melany Nicole Aguilar Ramirez

Resumen

La atrazina es uno de los herbicidas más efectivos y económicos del mundo, utilizado con más frecuencia que cualquier otro. Se detecta con frecuencia en el agua y se sabe que afecta la reproducción de la flora y fauna acuáticas, impactando la estructura de la comunidad en su conjunto. Además, las microalgas han sido reconocidas como uno de los microorganismos más eficientes para remediar efluentes industriales. Entre las microalgas, las diatomeas son eucariotas unicelulares con caparazones de sílice que se encuentran en todo tipo de cuerpos de agua y prosperan incluso en aguas residuales. Actúan como nanocontenedores inteligentes para adsorber varios metales traza, colorantes, polímeros y fármacos peligrosos para los humanos y la vida acuática. La hermosa nanoarquitectura de las diatomeas les permite unirse fácilmente a ligandos de elección para formar una estructura nanocompuesta con otras moléculas como metales, polímeros y otros contaminantes. Este trabajo estudia las propiedades estructurales y la adsorción de atrazina utilizando biosílice derivada de microalgas del género *Aulacoseira* decorada con nanopartículas de oro (Au-NPs) o nanopartículas de plata (Ag-NPs). La caracterización de las muestras se realizará utilizando espectroscopía ultravioleta-visible (UV-vis), espectroscopía infrarroja por transformada de Fourier (FTIR), espectroscopía Raman, microscopía electrónica de barrido (SEM), espectroscopía de dispersión de energía (EDX) y microscopía de fluorescencia. Este trabajo tiene como objetivo evaluar el uso de diatomeas decoradas con nanopartículas plasmónicas para eliminar la atrazina del agua residual. El impacto de este trabajo se basa en la importancia actual de la remediación ambiental utilizando recursos biológicos económicos, y estos nanomateriales de diatomeas naturalmente disponibles son económicos y altamente sensibles para ayudar en la fácil eliminación de contaminantes tóxicos del agua residual.

Palabras clave: Diatomeas, atrazina, nanopartículas, remoción, agua.

Abstract

Atrazine is one of the world's most effective and inexpensive herbicides and is used more frequently than any other herbicide. Atrazine is frequently detected in water and has been known to affect the reproduction of aquatic flora and fauna, impacting the community structure as a whole. Moreover, microalgae have been recognized as one of the most efficient microorganisms to remediate industrial effluents. Among microalgae, diatoms are silica-shelled unicellular eukaryotes found in all types of water bodies and flourish very well, even in wastewater. They act as smart nanocontainers to adsorb various trace metals, dyes, polymers, and drugs that are hazardous to humans and aquatic life. The beautiful nanoarchitecture in diatoms allows them to easily bind to ligands of choice to form a nanocomposite structure with other molecules such as metals, polymers, and other pollutants. This work studies the structural properties and the adsorption of atrazine using the *Aulacoseira genus* microalgae-derived biosilica decorated with gold nanoparticles (Au-NPs) or silver nanoparticles (Ag-NPs). The characterization of the samples will be done by using Ultraviolet-Visible spectroscopy (UV-vis), Fourier transforms infrared spectroscopy (FTIR), Raman spectroscopy, Scanning Electron Microscopy (SEM), Energy Dispersive spectroscopy (EDX), and Fluorescence microscopy. This work aims to evaluate the use of diatoms decorated with plasmonic nanoparticles to remove atrazine from wastewater. The impact of this work relies on the current importance of environmental remediation using low-cost bioresources, and such naturally available diatom nanomaterials are economical and highly sensitive to help in the facile removal of toxic pollutants from wastewater.

Keywords: Diatoms, atrazine, nanoparticles, removal, water.

Contents

List of Figures

List of Tables

Chapter 1

Introduction

Diatoms are a type of microalgae that play an important role in aquatic ecosystems, as they are a major component of the phytoplankton community[9]. They are unicellular organisms with unique silica cell walls, making them highly resistant to physical and chemical degradation. Due to their unique morphology, diatoms have been extensively studied for various applications, including biofuels, drug delivery, and environmental monitoring. Diatoms are a group of algae with a porous silica-based structure that can be functionalized for various applications, including water treatment[9]. They are abundant in aquatic environments and have been used to remove pollutants such as heavy metals, dyes, and organic compounds[10,11]. The unique properties of diatoms, such as their large surface area and porous structure, make them a suitable candidate for removing pollutants from water. One of the environmental issues of concern is the presence of pesticides in water bodies, which can adversely affect aquatic life and human health. Atrazine is a widely used herbicide found to be persistent in the environment and linked to various health issues, including cancer and reproductive problems. The increasing use of pesticides in agriculture has led to environmental contamination, especially of water resources[12,13]. One of the most commonly used herbicides is atrazine, which has been reported to have adverse effects on human health and the environment[14].

Atrazine is highly soluble in water and easily leaches into groundwater, a significant drinking water source[15]. Its high solubility and persistence make it difficult to remove from the environment[16]. Therefore, there is a need to develop efficient methods for its removal from water. Metal nanoparticles have been shown to be effective adsorbents for atrazine and can be used in water treatment to remove this harmful herbicide. Due to their high surface area and unique morphology, there has been growing interest in using diatoms doped with nanoparticles for water treatment applications. Nanoparticles for water treatment have gained significant attention in recent years[17]. Nanoparticles have unique physicochemical properties that effectively remove pollutants from water[9]. They can be synthesized with high specific surface area, charges, shapes and sizes, enhancing their adsorption capacity[18]. The incorporation of gold and silver nanoparticles into diatoms can further enhance their adsorption properties.

The aim of this work is to study the adsorption properties of diatoms decorated with gold and silver nanoparticles for atrazine removal from water. The project involved the synthesis of silver and gold nanoparticles and their decoration onto the diatom surface. The synthesized materials were characterized using UV-Vis spectroscopy,

scanning electron microscopy (SEM), Fourier Transform infrared spectroscopy (FTIR), and Raman spectroscopy. The adsorption properties of the synthesized materials are studied by conducting batch experiments and the effect of various parameters, such as pH and contact time. The results obtained from this study provides insights into the use of diatoms doped with nanoparticles for atrazine removal from water and will have important implications for the development of efficient water treatment methods. In addition to this research, it is also discussed the usage of these diatoms as biosensors in order to detect atrazine in water using Raman Analysis and Fluorescence microscopy. We aim to investigate the potential of diatoms decorated with metal nanoparticles for atrazine adsorption. Specifically, we synthesized diatoms doped with gold nanoparticles (AuNPs) and silver nanoparticles (AgNPs) to evaluate their adsorption capacity for atrazine.

This work is organized as follows. Chapter 2 provides the motivation for the present work, including the problem statement and objectives; then, Chapter 3 covers a theoretical background on diatoms, silver and gold nanoparticles for water treatment. Chapter 4 describes the methodology used in this study, including the synthesis of diatoms doped with nanoparticles, the evaluation of their adsorption capacity, and a brief description of characterization techniques used. Chapter 5 presents the results of this study, including the effect of various factors on the adsorption capacity of diatoms doped with nanoparticles. Finally, Chapter 6 presents the conclusions and recommendations for future research.

Chapter 2

Motivation

2.1 Problem Statement

The presence of pesticides in water bodies has become a major environmental concern, as they can have harmful effects on aquatic organisms and human health. Atrazine is one of the most commonly used herbicides worldwide and has been found to contaminate water sources. Therefore, there is a need for effective and sustainable methods to remove atrazine from water. Diatoms have shown potential for use in water treatment due to their high surface area and porous structure. However, the efficiency of diatoms for atrazine removal can be enhanced by decorating them with plasmonic nanoparticles as an effective adsorbent for atrazine removal from water.

2.2 General and Specific Objectives

2.2.1 General Objective

To study the atrazine adsorption using natural diatoms loaded with gold (AuNPs) or silver nanoparticles (AgNPs) for water treatment.

2.2.2 Specific Objectives

- Synthesis of gold and silver nanoparticles by the reduction and thermal decomposition methods, respectively.
- Decoration of diatom frustules with the synthesized silver or gold nanoparticles.
- Characterization of the samples using Raman spectroscopy, UV-Vis spectroscopy, SEM, and FTIR.
- Study the adsorption of atrazine on diatoms decorated with silver or gold nanoparticles.

Chapter 3

Theoretical Background

3.1 Diatoms

Diatoms are a diverse group of unicellular photosynthetic organisms that are present in virtually all aquatic environments. These organisms are unique in their intricate cell walls, which are composed of silica and exhibit various geometric shapes and structures. Diatoms are important primary producers in aquatic food webs and play a significant role in global biogeochemical cycles, such as the carbon and silicon cycles[19,20]. Moreover, diatoms have been widely used as bioindicators for monitoring water quality and environmental changes[21,22].

3.1.1 Taxonomy

Diatoms belong to the phylum Bacillariophyta, which is one of the most diverse and ecologically significant groups of algae. This phylum comprises approximately 10,000 species and 200 genera, which are classified based on their morphological characteristics and genetic diversity[23]. Diatoms are further divided into two classes: the centric diatoms (Coscinodiscophyceae) and the pennate diatoms (Bacillariophyceae)[21]. Centric diatoms are characterized by their radial symmetry, and their cell walls are typically circular or oval in shape. They are found in both marine and freshwater environments, where they play an essential role in primary production and carbon export[20]. On the other hand, pennate diatoms are bilaterally symmetrical, with elongated or rectangular cell walls. They are more diverse than centric diatoms and are found in various habitats, including freshwater, marine, and terrestrial environments[21].

3.1.2 Morphology

Diatom cell walls, also known as frustules, are composed of two overlapping silica valves that encase the cell's cytoplasm. The frustules exhibit various patterns, shapes, and sizes, which have been used as taxonomic features to differentiate between species[21]. Some diatoms have intricate structures, such as spines, pores, and ribs, which are thought to provide mechanical support, regulate nutrient uptake, and increase surface area for gas exchange[19].

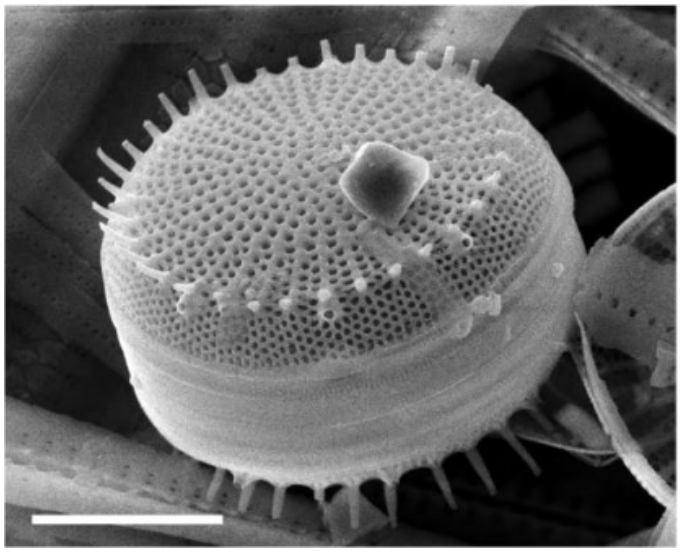

Figure 3.1: Complete Stephanodiscus minutulus frustule. Both valves and girdle bands comprising the "pill box" architecture are visible. Scale bar equals 5 um. Adapted from Smol, et al[1]

Diatoms also exhibit various sizes, ranging from a few micrometers to several hundred micrometers. The smallest diatoms are unicellular and can only be observed under an optical or electronic microscope, while larger diatoms can form chains or colonies visible to the naked eye[21]. The size of diatoms is an important factor that affects their physiology, ecology, and biogeochemistry, as larger diatoms have a higher sinking rate and contribute more to carbon export than smaller ones[20].

3.1.3 Physiology

Diatoms are photosynthetic organisms that use chlorophyll a and c as their primary pigments. They also contain accessory pigments, such as fucoxanthin and diadinoxanthin, which absorb light at different wavelengths and allow diatoms to harvest light more efficiently in different environmental conditions[20]. Diatoms are unique in their ability to perform a form of carbon fixation known as the C4 pathway, which allows them to efficiently concentrate carbon dioxide around the enzyme responsible for carbon fixation[24]. This adaptation enables diatoms to thrive in environments with low carbon dioxide concentrations, such as the open ocean, where they play a crucial role in the biological pump that transfers carbon from the surface to the deep ocean[20]. In addition to their photosynthetic abilities, diatoms are also known for their remarkable silica metabolism. Diatoms can take up silicon from the environment and use it to build their intricate cell walls, which are composed of amorphous silica[19]. The process of silica deposition is highly regulated, involving multiple enzymes and transporters, and is thought to be tightly linked to the cell cycle and cell division[25]. Silica deposition in diatoms is an active area of research, as it has significant implications for understanding biomineralization and biotechnology applications[26].

3.1.4 Ecology

Diatoms are ubiquitous in aquatic environments, and various environmental factors, including light, nutrients, temperature, and salinity, influence their distribution and abundance. Diatoms are often found in high numbers in nutrient-rich environments, such as up-welling zones and estuaries, where they can form dense blooms that contribute to oxygen depletion and harmful algal blooms[27]. On the other hand, diatoms are also found in oligotrophic environments, such as the open ocean, where they contribute to most primary production and carbon export[20]. Diatoms play a crucial role in the aquatic food web, serving as the base of the food chain for many aquatic organisms, including zooplankton, fish, and marine mammals. Diatoms are known to produce various lipids and polysaccharides, which are important food sources for grazers and can also contribute to the formation of marine snow, a key component of the biological pump[20].

3.1.5 Biogeochemistry

Diatoms have significant implications for global biogeochemical cycles, including the carbon and silicon cycles. Diatoms are responsible for approximately 20 % of global primary production, and their role in carbon sequestration and export is well established[20]. Diatoms are known to export carbon to the deep ocean through the biological pump, where it can be stored for thousands of years, making diatoms a critical component of the global carbon cycle[19]. Diatoms also play a significant role in the silicon cycle, as they are responsible for most silica deposition in the ocean. Silica is a limiting nutrient in many marine environments, and diatoms can play a crucial role in regulating silica availability and cycling[28]. The formation and dissolution of diatom frustules can affect silica availability and storage in the ocean, which has significant implications for the biogeochemistry of silicon[29].

3.1.6 Diatom *Aulacoseira* genus used in this work

The *Aulacoseira* genus is a freshwater diatom species that is characterized by its distinct morphology. The cells are cylindrical and have a characteristic granulated surface. The valves are elliptical, and the central area is raised, forming a distinct central nodule. The species is known to form long chains resulting from the presence of linking spines[30]. These spines are also present on the valve surface and help attach adjacent cells. Studies have shown that *Aulacoseira* species, including the *Aulacoseira* genus, play an important role in freshwater ecosystems. Additionally, *Aulacoseira* species are known to be sensitive to changes in environmental conditions, including changes in temperature, pH, and nutrient levels[31]. Therefore, they are often used as water quality indicators in freshwater systems. The *Aulacoseira* species found in the Guayllabamba River have recently been studied for drug delivery[32] and also for the photodegradation of some dyes in water[33].

3.2 Atrazine

Atrazine is a widely used herbicide in the triazine class of pesticides. It is one of the most commonly detected contaminants in surface and groundwater and has been detected in more than half of the drinking water wells tested

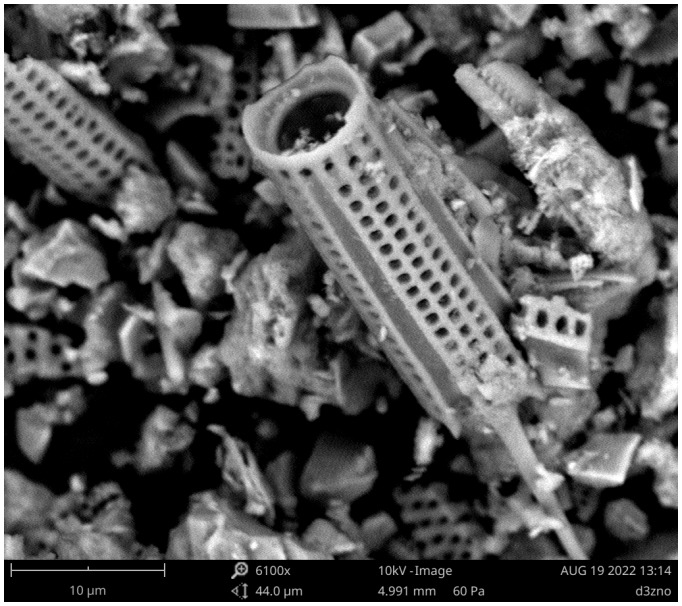

Figure 3.2: SEM micrograph of *Aulacoseira* genus type diatom obtained in this work.

in the United States[34]. Atrazine has been the subject of significant scientific research due to its potential to cause environmental and human health problems. This section aims to provide a theoretical background of atrazine, including its chemistry, environmental fate, and human health effects.

3.2.1 Chemical Properties

Atrazine, 2-chloro-4-ethylamino-6-isopropylamino-s-triazine, has the chemical formula $C_8H_14ClN_5$. It is a white, crystalline solid that is soluble in water and organic solvents such as acetone, ethanol, and chloroform[35]. The herbicide is relatively stable in neutral and alkaline environments but can undergo hydrolysis in acidic conditions to form hydroxyatrazine, a more toxic metabolite[36]. The primary mode of action of atrazine is to inhibit photosynthesis in plants by binding to the D1 protein of photosystem II[36]. The herbicide is effective against a broad range of weeds and is particularly useful for controlling grasses and broadleaf weeds in corn and sorghum crops[34].

3.2.2 Environmental Fate

Atrazine is applied to agricultural fields as a preemergent or postemergent herbicide and can also be used on residential lawns and golf courses[34]. The herbicide can enter surface water and groundwater through runoff and leaching and can persist in the environment for several months to years[37]. In soil, atrazine is subject to adsorption, degradation, and leaching. The herbicide has a low adsorption coefficient, so it can easily move through soil and leach into groundwater[37]. Degradation of atrazine in the soil is primarily mediated by soil microorganisms, which can break

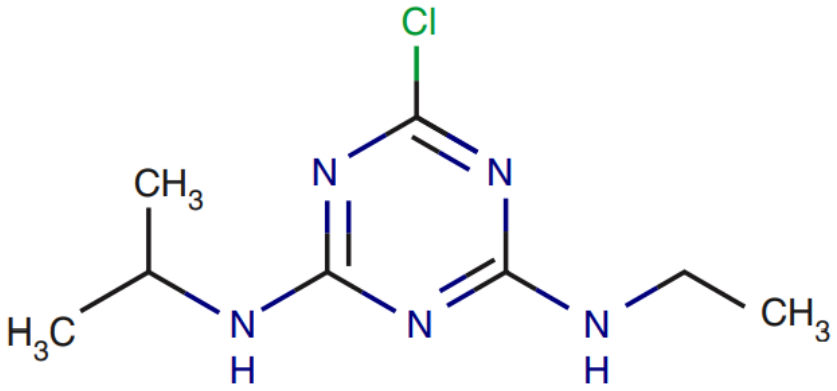

Figure 3.3: Atrazine chemical structure.

down the herbicide into less toxic compounds such as hydroxyatrazine, deethylatrazine, and deisopropylatrazine[36]. The atrazine degradation rate in the soil depends on factors such as soil pH, temperature, and moisture content[37]. In surface water, atrazine can undergo photodegradation, hydrolysis, and microbial degradation[36]. Photodegradation is the primary degradation pathway in surface water and it can be accelerated by the presence of dissolved organic matter and sunlight[34]. Hydrolysis of atrazine in water can produce hydroxyatrazine, a more toxic metabolite, and dealkylated products[36]. Microbial degradation of atrazine in water is slower than in soil, and it depends on factors such as temperature, pH, and nutrient availability[34]. Atrazine has been detected in surface water and groundwater across the United States, with higher levels of contamination observed in agricultural areas[34]. This herbicide has been found in streams, rivers, lakes, and drinking water wells. In some cases, atrazine contamination has been linked to adverse effects on aquatic ecosystems, including decreased plant and animal diversity[37].

3.2.3 Human Health Effects

Atrazine has been the subject of significant concern due to its potential to cause adverse human health effects. The herbicide has been classified as a possible human carcinogen by the International Agency for Research on Cancer (IARC)[38]. Additionally, atrazine has been linked to developmental and reproductive toxicity and endocrine disruption[34]. Studies have shown that exposure to atrazine can lead to adverse effects on the male reproductive system, including decreased sperm count, altered hormone levels, and reduced fertility[39]. Atrazine has also been linked to an increased risk of breast cancer, particularly in postmenopausal women[34]. In animal studies, atrazine exposure has been shown to cause birth defects and developmental delays[39]. Endocrine disruption is one of the most well-documented effects of atrazine exposure. The herbicide has been shown to interfere with the hormonal system, leading to altered reproductive function, decreased immune function, and behavioral changes[34]. Atrazine can bind to the estrogen receptor, leading to increased estrogenic activity and potentially contributing to the development of breast cancer[36]. In addition to its potential human health effects, atrazine has been shown to have adverse effects on

non-target organisms, including amphibians, fish, and aquatic invertebrates[34]. The herbicide can disrupt the growth and development of these organisms, leading to decreased population sizes and decreased biodiversity.

3.2.4 Potential impacts of atrazine contamination

Atrazine contamination can have significant negative impacts on ecosystems and human health. In aquatic ecosystems, atrazine can cause harm to fish, amphibians, and aquatic reptiles and alter the structure and function of aquatic communities[35]. Atrazine has also been shown to cause endocrine disruption in wildlife, leading to reproductive abnormalities and feminization of male gonads[39]. In addition to its effects on wildlife, atrazine can also pose a risk to human health. The International Agency for Research on Cancer[38] has classified atrazine as a possible human carcinogen. Additionally, studies have shown that exposure to atrazine can adversely affect human reproductive and developmental health[34]. Atrazine exposure has been associated with an increased risk of preterm birth, low birth weight, and fetal growth restriction[34].

3.3 Nanoparticles

Nanoparticles have been widely studied in the past decades due to their unique physical and chemical properties. Silver (Ag) and gold (Au) nanoparticles have received considerable attention due to their potential applications in various fields, including electronics, medicine, and catalysis. In recent years, their application as herbicide adsorbents has been extensively explored[40–42]. Herbicides are chemicals used to control unwanted plants in agricultural and other settings. They are among the most widely used pesticides in the world, with approximately 2.6 million tons used annually[43]. However, the excessive use of herbicides can lead to several environmental issues, such as groundwater contamination, toxicity to non-target organisms, and the development of herbicide-resistant weeds[44,45]. One way to mitigate these issues is using nanoparticles as herbicide adsorbents. The use of nanoparticles in adsorption processes provides several advantages, including high surface area, high adsorption capacity, and the ability to tune their surface chemistry to adsorb target molecules selectively[46]. Silver and gold nanoparticles, in particular, have shown promising results as herbicide adsorbents due to their unique physicochemical properties[47,48].

3.3.1 Silver Nanoparticles

Silver nanoparticles (AgNPs) have a high surface-to-volume ratio, which enhances their reactivity and makes them suitable for various applications, including the adsorption of herbicides. AgNPs have been reported to adsorb a wide range of herbicides, including atrazine, glyphosate, and paraquat, among others[45]. The adsorption process is mainly due to the electrostatic interaction between the negatively charged herbicide molecules and the positively charged surface of the AgNPs[46]. Several factors affect the adsorption capacity of AgNPs, such as size, shape, concentration, and surface chemistry. For instance, it has been shown that the adsorption capacity of AgNPs increases with decreasing particle size due to the increased surface area available for adsorption[49]. Additionally, the adsorption capacity can be enhanced by modifying the surface chemistry of AgNPs through functionalization with various organic or inorganic moieties[46].

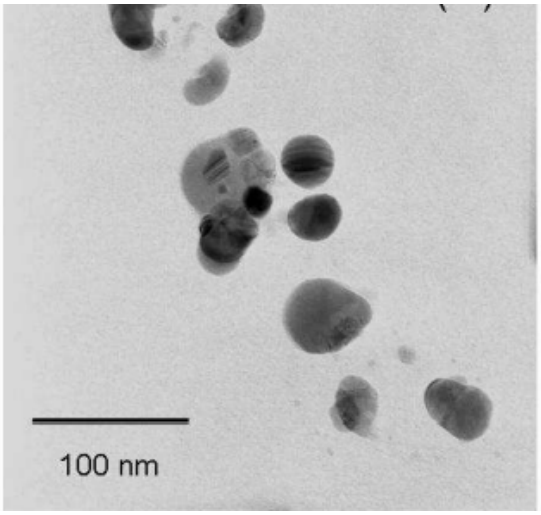

Figure 3.4: TEM image of spherical silver nanoparticles obtained at 2.0 mM of citrate of sodium solution retireved from Guzman, et al[2].

3.3.2 Gold Nanoparticles

Gold nanoparticles (AuNPs) have also been investigated for their potential application as herbicide adsorbents. AuNPs have a high surface area and can be functionalized with various functional groups, making them highly selective for specific herbicides. The adsorption of herbicides by AuNPs is can occur through various mechanisms, including the formation of hydrogen bonds between functional groups on the nanoparticle surface and the herbicide molecules. However, the adsorption process is complex and can involve multiple interactions between the herbicide and the nanoparticle surface that include electrostatic interactions and van der Waals forces.[42]. The size and shape of AuNPs also play a critical role in their adsorption capacity. For instance, it has been reported that AuNPs with a size range of 20-50 nm show the highest adsorption capacity for atrazine, whereas smaller or larger particles exhibit a lower adsorption capacity[43].

3.4 Nanocomposites

Nanocomposites comprise a bulk material and nanosized particles dispersed throughout the matrix[50]. Incorporating nanoparticles into a bulk material can enhance its mechanical, thermal, and electrical properties and improve its chemical and biological properties[51]. These materials can potentially be used in a wide range of applications, including biomedical, electronic, and environmental applications[52].

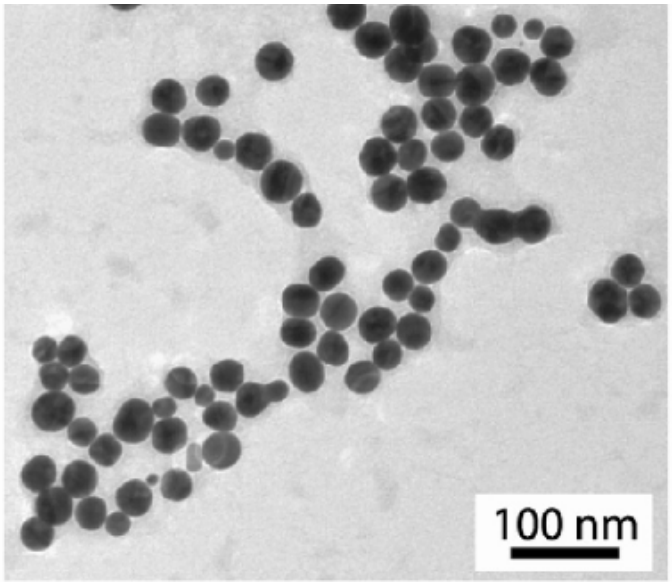

Figure 3.5: TEM micrograph of gold nanoparticles using CTAB. Retrieved from Smith, et al[3].

3.4.1 Synthesis of Nanocomposites

Nanocomposites can be synthesized through various methods, such as in-situ polymerization, melt mixing, solution mixing, and electrospinning[53]. In-situ polymerization involves the incorporation of nanoparticles into the polymer matrix during the polymerization process[52]. Melt mixing involves mixing the polymer and nanoparticles in the molten state, followed by cooling and solidification[54]. Solution mixing involves mixing the polymer and nanoparticles in a solvent, followed by solvent evaporation[50]. Electrospinning involves using an electric field to generate a nanofiber composed of the polymer and nanoparticles[55].

3.4.2 Characterization of Nanocomposites

The characterization of nanocomposites is important to understand their properties and performance. Several techniques are used to characterize nanocomposites' structure, morphology, and properties, such as X-ray diffraction, transmission electron microscopy, scanning electron microscopy, and thermal analysis[55]. X-ray diffraction is used to determine the crystalline structure of the nanoparticles and the polymer matrix[56]. Transmission electron microscopy and scanning electron microscopy are used to visualize the nanoparticles' size, shape, and dispersion in the polymer matrix[54]. Thermal analysis techniques, such as differential scanning calorimetry and thermogravimetric analysis, are used to determine the thermal properties of the nanocomposites, such as the glass transition temperature and thermal stability[53].

3.4.3 Applications of Nanocomposites

Nanocomposites have a wide range of applications due to their unique properties. In biomedical applications, nanocomposites can be used for drug delivery, tissue engineering, and medical implants[51]. In electronic applications, nanocomposites can be used in sensors, transistors, and solar cells[53]. In environmental applications, nanocomposites can be used for water treatment, air purification, and pollution remediation[52].

3.5 Material Absorption

Absorption is the process by which molecules are taken up by a bulk phase, such as a liquid or solid[57]. This process can occur through various mechanisms, including dissolution, chemical reaction, and physical adsorption. The rate of absorption depends on a number of factors, including the properties of the absorbing material, the properties of the absorbed molecule, and the conditions of the environment.[58,59]

Mechanisms of Absorption

The absorption mechanism depends on the nature of the absorbing phase and the absorbed molecule. Absorption can generally occur through dissolution, chemical reactions, and physical adsorption. Dissolution is the process by which a solute (absorbed molecule) is taken up by a solvent (absorbing phase) to form a homogeneous solution[58]. The absorption rate is influenced by the solubility of the solute in the solvent and the concentration gradient of the solute across the interface between the two phases. A chemical reaction involves the formation of a chemical bond between the absorbed molecule and the absorbing phase[60,61]. This mechanism often removes contaminants from a liquid or gas phase. For example, activated carbon is often used to remove organic contaminants from water by chemically binding the contaminants to the carbon surface[61,62].

Factors Influencing Absorption

The absorption rate is influenced by several factors, including the properties of the absorbing phase and the absorbed molecule and the conditions of the environment[57]. The following are some of the most important factors influencing absorption:

Surface Area

The surface area of the absorbing phase is an important factor in absorption. A greater surface area provides more opportunities for the absorbed molecule to come into contact with the absorbing phase, increasing the absorption rate. This is why porous materials like activated carbon are often used for absorption applications[63].

Porosity

The porosity of the absorbing phase is also important in absorption. A high degree of porosity provides more surface area for absorption but can also result in a reduced absorption capacity due to the presence of pores that are too large

to trap the absorbed molecule[64] effectively. Therefore, the size and distribution of the pores in the absorbing phase must be carefully controlled to maximize absorption efficiency.[57]

Concentration Gradient

The concentration gradient of the absorbed molecule across the interface between the absorbing phase and the environment also influences absorption[59]. A greater concentration gradient results in a higher absorption rate, as the absorbed molecule moves from an area of high concentration to an area of lower concentration. Therefore, the concentration of the absorbed molecule in the environment must be carefully controlled to maximize absorption efficiency.[60]

3.5.1 Applications of Absorption

Absorption is used in various practical applications, including gas storage, separation processes, and drug delivery. Some of the most common applications are discussed below.

Gas Storage

Absorption stores gases, such as hydrogen, methane, and carbon dioxide[64]. Due to their high surface area and porosity, porous materials, such as zeolites and metal-organic frameworks, are often used as absorbing phases for gas storage applications. The absorbed gas can be released by reducing the pressure or increasing the temperature, making it a useful method for storing and transporting gases.[58]

Separation Processes

Absorption is also used in the separation and purification of gases and liquids. For example, activated carbon is often used to remove organic contaminants from water, while silica gel is used to remove moisture from air[65]. In gas separation, selective absorption can be used to separate a specific gas from a mixture. This is commonly used in natural gas processing to separate methane from other gases.[62]

Drug Delivery

Absorption is used in the delivery of drugs, particularly for drugs that are poorly soluble in water or have poor bioavailability[57]. Solid lipid nanoparticles, liposomes, and micelles are often used as absorbing phases for drug delivery applications. The drug is absorbed into the absorbing phase and then delivered to the target site in the body.[32]

3.6 Material Adsorption

Adsorption is the process by which molecules are attached to the surface of a solid. This process occurs through weak intermolecular forces, such as van der Waals forces, hydrogen bonding, and electrostatic interactions.[64] The rate and extent of adsorption depend on a number of factors, including the properties of the adsorbent, the properties of the adsorbate, and the conditions of the environment.[63]

3.6.1 Mechanisms of Adsorption

Adsorption occurs through a variety of mechanisms, including physisorption and chemisorption.[65] Physisorption is a weak interaction between the adsorbate and the adsorbent surface and is driven by van der Waals forces. Chemisorption involves the formation of a chemical bond between the adsorbate and the adsorbent surface and is driven by electron transfer or sharing between the adsorbate and the adsorbent surface[62,64].

3.6.2 Factors Influencing Adsorption

The rate and extent of adsorption are influenced by a variety of factors, including the properties of the adsorbent and the adsorbate, as well as the conditions of the environment.[58]

Surface Area and Porosity

The surface area and porosity of the adsorbent are important factors in adsorption.[60] A higher surface area and greater porosity result in more available surface sites for adsorption, leading to a higher rate and extent of adsorption. Therefore, porous materials such as activated carbon and silica gel are commonly used as adsorbents in adsorption processes.[59]

3.6.3 Applications of Adsorption

Adsorption is used in various practical applications, including gas and liquid purification, separation processes, and catalysis. Some of the most common applications are discussed below.[58]

Gas and Liquid Purification

Adsorption is used to purify gases and liquids by removing impurities[33] such as volatile organic compounds, sulfur compounds, and nitrogen oxides. Activated carbon, zeolites, and silica gel are commonly used as adsorbents for gas and liquid purification applications.[57]

Separation Processes

Adsorption is also used in separation processes, such as chromatography and ion exchange. In chromatography, adsorbents with specific chemical properties are used to separate molecules based on their affinity for the adsorbent

surface. In ion exchange, adsorbents with specific charges are used to separate ions based on their charge.[65]

Catalysis

Adsorption is also used in catalysis, where the adsorbent surface is used to hold the reactant molecules in close proximity to each other, promoting the formation of the desired product. For example, metal catalysts such as platinum and palladium are often used as adsorbents in catalytic reactions.[66]

3.7 Diatoms Mechanism of Adsorption and Absorption

Adsorption and absorption are two distinct processes that diatoms use to take up substances from their surroundings. Adsorption refers to surface process involving the attachment of molecules or particles to the surface of a material by a chemical or physical interactions, while absorption involves the penetration of molecules or particles into the bulk of a material. In diatoms, these processes are governed by the unique structure of their cell wall, which is composed of two overlapping halves or valves made of amorphous silica[67].

The surface of the diatom cell wall is covered with various functional groups, including hydroxyl, carboxyl, and amine groups, which can form hydrogen bonds, electrostatic interactions, and van der Waals forces with surrounding molecules or particles[68]. These functional groups are also responsible for diatom cells' high surface area-to-volume ratio, making them efficient adsorbents[67]. On the other hand, absorption in diatoms occurs through the penetration of molecules or particles into the pores or channels in the diatom cell wall[69]. The diatom cell wall has a complex three-dimensional structure consisting of various pores and channels, including large central pores, radial channels, and areolae[67]. These pores and channels allow for the diffusion of substances into and out of the diatom cell.

3.7.1 Factors Affecting Adsorption and Absorption in Diatoms

The efficiency of adsorption and absorption in diatoms is affected by various factors, including the size and shape of the molecules or particles, the concentration of the substances in the environment, and the properties of the diatom cell wall. For example, small molecules and particles are more easily adsorbed and absorbed by diatoms than larger ones[68]. Similarly, the concentration of the substances in the environment affects their uptake by diatoms, with higher concentrations leading to increased adsorption and absorption[69]. The properties of the diatom cell wall also play an important role in the efficiency of adsorption and absorption. As mentioned earlier, the surface area-to-volume ratio of diatom cells is a crucial factor in their ability to adsorb substances from their environment[67]. The size and shape of the pores and channels in the diatom cell wall also influence absorption efficiency. For example, larger pores and channels allow for the diffusion of larger molecules and particles, while smaller ones are more selective and only allow for the diffusion of smaller substances[67].

The chemical composition of the diatom cell wall is another important factor in the efficiency of adsorption and absorption. The surface functional groups, such as hydroxyl, carboxyl, and amine groups, are crucial in forming bonds with surrounding molecules and particles[68]. The distribution of these functional groups across the diatom cell wall can also affect the selectivity of the adsorption process. For example, if the functional groups are distributed

unevenly across the cell wall, the adsorption of certain substances may be favored over others[69]. Temperature, pH, and salinity are other environmental factors that can affect the efficiency of adsorption and absorption in diatoms. These factors can influence the diatom cell wall's chemical composition and the surrounding environment's properties, thereby affecting the interactions between diatoms and surrounding substances[67].

3.7.2 Applications of Diatoms in Adsorption and Absorption

The unique properties of diatoms make them valuable materials for various applications in adsorption and absorption of contaminants in water. One of the most promising applications is developing biofilters for water treatment. Diatoms have efficiently removed various contaminants from water, including heavy metals, organic compounds, and microorganisms[70]. The high surface area-to-volume ratio of diatoms, combined with their ability to adsorb certain substances selectively, makes them effective in removing specific contaminants from water.

Diatoms have also been used in the development of biosensors for the detection of environmental pollutants. The functional groups on the surface of diatom cells can be modified to specifically interact with certain pollutants, allowing for their selective detection[71]. In addition to environmental applications, diatoms have also been explored for their potential in drug delivery systems. The porous structure of the diatom cell wall allows for the encapsulation of drugs, which can then be released in a controlled manner[72]. The biocompatibility of diatoms also makes them attractive candidates for use in biomedical applications.

3.8 Adsorption Kinetics Models

Adsorption is a surface process where molecules from a gas or liquid (called the adsorptive) adhere to a solid surface.[73] In practice, adsorption is carried out as an operation, whether in a batch process or continuously, within a column filled with porous sorbents. In these situations, it is important to consider mass transfer effects, which are bound to occur. The entire adsorption process involves mass transfer and consists of four stage. Including the transport of the adsorbate to the outer surface of the adsorbent, external film diffusion (concerned with the movement of the adsorbate through a stationary layer around the particle), internal (pore) diffusion or intraparticle diffusion (involving the transfer of the adsorbate from the particle's surface to the active sites within its porous structure), and adsorption, where the adsorbate adheres to available sites on the adsorbent's surface. It's worth noting that the rate-limiting step typically revolves around adsorbate transport to the adsorbent under appropriate conditions, but adjustments in process parameters can shift the limiting stage to intraparticle diffusion or emphasize the interaction between the adsorbate and the adsorbent.[74,75]

The effective planning and expansion of an adsorption system implies a deep understanding of both adsorption equilibrium and the dynamics involved.[76] The comprehension of kinetics is often constrained by the intricate theoretical aspects of adsorption mechanisms. Numerous models with differing levels of complexity have been created to forecast how quickly an adsorbate is taken up by an adsorbent. Among these models, the pseudo-first-order (PFO) and pseudo-second-order (PSO) models are the most frequently employed empirical models in the study of liquid adsorption research and these are the ones used in this thesis.[76,77]

3.8.1 Pseudo First Order Kinetic Model

The equation for pseudo-first order kinetics was introduced at the first time by Lagergren[74]. This model assumes that the rate of adsorption is directly proportional to the number of unoccupied adsorption sites on the adsorbent. The equation is as follows:

$$\frac{dQ}{dt} = k_1.(Q_e - Q_t) \tag{3.1}$$

where Q_t is the adsorption capacity (mg/g), Q_e is the equilibrium adsorption capacity (mg/g); t is the time (min) and k_1 = rate constant (min^{-1}). It is generally used in the linearized form proposed by Ho and McKay[73]:

$$ln(Q_e - Q_t) = lnQ_t - k_1 t \tag{3.2}$$

To calculate the pseudo-first order rate constant (k_1), it is performed a linear regression analysis on a plot of $ln(Q_e - Q_t)$ against t. The slope of the linear plot give us k_1.

3.8.2 Pseudo Second Order Kinetic Model

The pseudo-second-order (PSO) model, which relies on the equilibrium adsorption capacity, is frequently employed due to its clear ability to accurately represent experimental data[74]. This model assumes that the rate of adsorption is directly proportional to the square of the number of unoccupied adsorption sites on the adsorbent. The equation is as follows:

$$\frac{dQ}{dt} = k_2.(Q_e - Q_t)^2 \tag{3.3}$$

where k_2 is the pseudo-second-order (PSO) rate constant. Other values are labeled as the previous model mentioned. Integrating with the previous equation with initial conditions of $Q_t = 0$ when t = 0 and subsequent rearrangement obtains the linearized form:

$$\frac{t}{Q_t} = \frac{1}{k_2 Q_e^2} + \frac{t}{Q_e} \tag{3.4}$$

To calculate the pseudo-second order rate constant (k_2), it can be performed a liner regression analysis on a plot of t/Q_t against t. The slope of the linear plot give us k_2.

Most of environmental adsorption studies fit the pseudo first order and pseudo second order models to the same set of kinetic data. Better fits are determined using the statistical least squares method from the linear regression from each model with the experimental data. Under controlled reactions, the rate constants (k_1 and k_2, respectively, for pseudo first order and pseudo second order) are regarded as reaction rate constants.[73] This models are useful to evaluate adsorption process, even though it is needed strong knowledge of the origins, strengths, and limitations of these models according with Tan, et al.[74] And also said that the model parameters are empirical constants that have no distinct theoretical significance.[74]

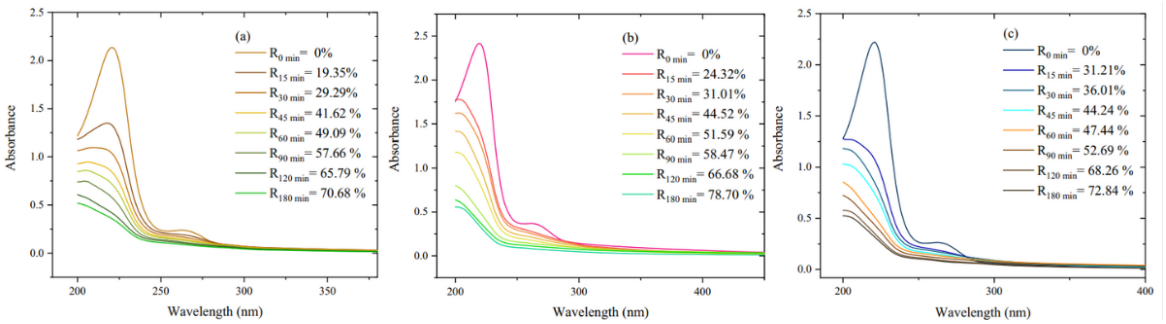

Figure 3.6: Absorbance spectra for the atrazine removal in water samples of **a** Conceição, **b** Jacuí, and **c** Soturno rivers. Adapted from Netto, et al[4].

3.9 Characterization Techniques

3.9.1 UV-Vis Spectroscopy

UV-vis spectroscopy is a widely used analytical technique that measures molecules' absorption of ultraviolet (UV) and visible (vis) light. The principle behind UV-vis spectroscopy lies in the interaction of light with electronic transitions of molecules. When molecules are exposed to UV or visible light, electrons within the molecule may absorb photons and transit from their ground state to higher energy electronic states. The energy difference between the ground and excited states corresponds to specific wavelengths of light, resulting in characteristic absorption bands in the UV-vis spectrum. By analyzing the absorption patterns, valuable information about the sample's molecular structure, concentration, and chemical environment can be obtained[78,79].

One of the fundamental aspects of UV-vis spectroscopy is the Beer-Lambert Law, which provides a quantitative relationship between the absorbance, the concentration of the absorbing species, and the path length of the sample. The law is expressed as $A = \varepsilon \cdot c \cdot l$, where A is the absorbance, ε is the molar absorptivity or molar extinction coefficient, c is the concentration of the analyte, and l is the path length of the sample cell. This linear relationship allows for the accurate determination of analyte concentrations by measuring absorbance at specific wavelengths and constructing calibration curves.[78–80].

UV-vis spectrophotometers consist of a light source, a monochromator or a grating to select the desired wavelength, a sample holder or cuvette, and a detector to measure the intensity of transmitted or absorbed light. Modern UV-vis spectrophotometers often incorporate advanced features such as automatic wavelength scanning, multiple path length options, and computerized data analysis. Researchers rely on UV-vis spectroscopy to study molecular properties, monitor enzymatic reactions, analyze metal ion complexes, characterize nanoparticles, and determine the purity of chemical compounds[80,81]. In figure 3.6 it can be observed a sample of UV-vis spectra, retrieved from Netto, et al[4].

3.9.2 Scanning Electron Microscopy (SEM)

Scanning Electron Microscopy (SEM) is a versatile and powerful imaging technique widely employed for high-resolution characterization of surfaces and materials. The fundamental principle of SEM involves scanning a focused electron beam over a sample's surface and detecting the emitted secondary electrons, backscattered electrons, or characteristic X-rays. The interaction between the incident electrons and the sample generates signals that provide information about the sample's topography, composition, and morphology. SEM offers exceptional spatial resolution, enabling the visualization of nanoscale features and surface structures. The technique is particularly valuable for studying samples with complex geometries, ranging from biological specimens to engineered materials, and has become an indispensable tool in various scientific and industrial fields[82,83].

The application of Scanning Electron Microscopy (SEM) holds great significance in characterizing diatoms doped with nanoparticles. Diatoms are intricate microalgae with intricate and unique silica-based cell walls, known as frustules, that exhibit intricate nanostructures. Incorporating nanoparticles into diatom frustules imparts new properties and functionalities, making them promising candidates for various applications, including sensing, catalysis, and drug delivery. SEM allows researchers to visualize and analyze nanoparticle morphology and spatial distribution on diatom frustules. By obtaining high-resolution images and elemental mapping, SEM aids in assessing the uniformity, dispersion, and interactions of nanoparticles with diatom structures as it can be seen in the SEM micrographs example in Figure 3.7 retrieved from Pannico, et al[5]. This information is critical for understanding the composite's performance and optimizing its design for specific applications[84,85].

3.9.3 Energy Disperse X-Ray (EDX)

Energy Dispersive X-ray Spectroscopy (EDS) is a widely used analytical technique that provides valuable insights into the elemental composition of materials. EDS is typically integrated with scanning electron microscopy (SEM), allowing for simultaneous imaging and elemental analysis. The fundamental principle of EDS involves the interaction of a focused electron beam with a sample, resulting in the emission of characteristic X-rays. Each element in the sample emits unique X-ray energies as electrons transition from higher energy levels to lower ones. EDS detectors measure the energy and intensity of these X-rays, enabling the identification and quantification of the elements present in the sample. EDS is essential for investigating the spatial distribution of elements within a sample, facilitating detailed compositional analysis, and aiding in understanding material properties, phase identification, and chemical mapping[82,86].

The Energy Dispersive X-ray Spectroscopy (EDS) application holds significant promise for characterizing diatoms doped with nanoparticles. Diatoms, with their intricate silica-based cell walls, offer a unique platform for incorporating nanoparticles with potential functional enhancements. When coupled with SEM, EDS enables detecting and quantifying elements present within diatom structures. By analyzing the X-ray spectra emitted during electron-sample interactions, EDS facilitates the identification of elements within the diatom frustules and the nanoparticles. This information is crucial for confirming the successful incorporation of nanoparticles and understanding their distribution within the diatom matrix, as it can be seen in Figure 3.8 retrieved from Gutu, et al[6]. Additionally, EDS can aid in assessing any compositional changes or interactions occurring between the diatom

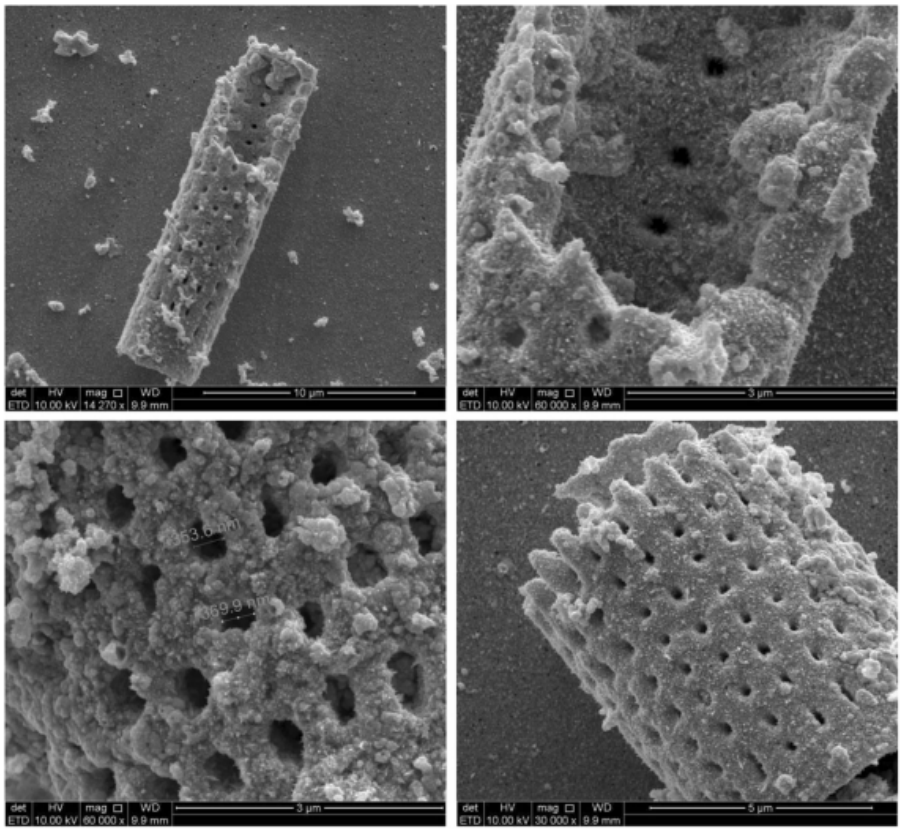

Figure 3.7: (**a**, up left) Single micrometric diatom frustule. (**b**, up right) Au nanoparticle covers homogeneously the outer and inner surfaces of the frustule. (**c**, down left) An enlargement of outer surface with pore size measurement. (**d**, down right) A smaller micrometric frustule. . Adapted from Pannico, et al[5].

frustules and the nanoparticles, contributing to a comprehensive characterization of the composite material[87,88].

3.9.4 Raman spectroscopy

Raman spectroscopy is a powerful analytical technique used to probe the vibrational modes of molecules. It is based on the inelastic scattering of monochromatic light, typically from a laser source, by a sample. When photons interact with molecules, a fraction of the scattered light gains or loses energy, resulting in a Raman shift corresponding to molecular vibrations. Raman spectra provide a fingerprint of the molecular composition, enabling the identification of functional groups and structural information. The intensity of Raman scattering is relatively weak, making it essential to employ advanced techniques like Surface-Enhanced Raman Spectroscopy (SERS) to enhance the signal and enable sensitive molecular analysis[89].

Surface-Enhanced Raman Spectroscopy (SERS) takes advantage of localized electromagnetic fields generated near nanostructured metal surfaces, such as gold or silver, to significantly amplify Raman signals as it can be seen in the figure 3.9 retrieved from Leon, et al[7]. In SERS, molecules adsorbed onto these surfaces experience enhanced Raman scattering due to the excitation of localized surface plasmon resonances. This phenomenon leads to immense signal enhancement, often reaching factors of 10^6 to 10^{14}, enabling the detection of trace molecules with high sensitivity. SERS has diverse applications, including chemical and biological sensing, environmental monitoring, and material characterization.[90,91].

The application of SERS for characterizing diatom doped with nanoparticles offers unique insights into composite materials. Diatoms, with their intricate silica frustules, provide a scaffold for incorporating nanoparticles, yielding functional hybrids with tailored properties. SERS can elucidate the interactions between the diatom frustules and the adsorbed molecules' spatial distribution and chemical environmentment of the adsorbed molecules. By leveraging the signal enhancement of SERS, researchers can detect and identify specific molecules even at low concentrations. This capability is particularly relevant for studying the interactions and behaviors of nanoparticles within the complex diatom structure[85].

3.9.5 Fourier Transform Infrared spectroscopy (FTIR)

Fourier-Transform Infrared (FTIR) spectroscopy is a versatile analytical technique widely utilized to characterize materials based on their vibrational modes. FTIR spectroscopy measures the interaction of infrared light with a sample, resulting in absorption, transmission, or reflection spectra. Molecules possess characteristic vibrational frequencies associated with their functional groups, and these frequencies manifest as specific absorption bands in the FTIR spectrum. FTIR provides valuable information about chemical bonds, molecular structure, and composition. FTIR spectroscopy is non-destructive, requires minimal sample preparation, and has applications across diverse fields, including chemistry, biology, materials science, and environmental analysis[92,93].

The application of FTIR spectroscopy plays a crucial role in characterizing diatoms doped with nanoparticles. Diatoms, with their intricate silica frustules, offer a unique substrate for nanoparticle incorporation. FTIR spectroscopy can elucidate changes in molecular vibrations resulting from the presence of nanoparticles within the diatom structure. Specific vibrational modes related to both diatom frustules and the nanoparticles can be identified and

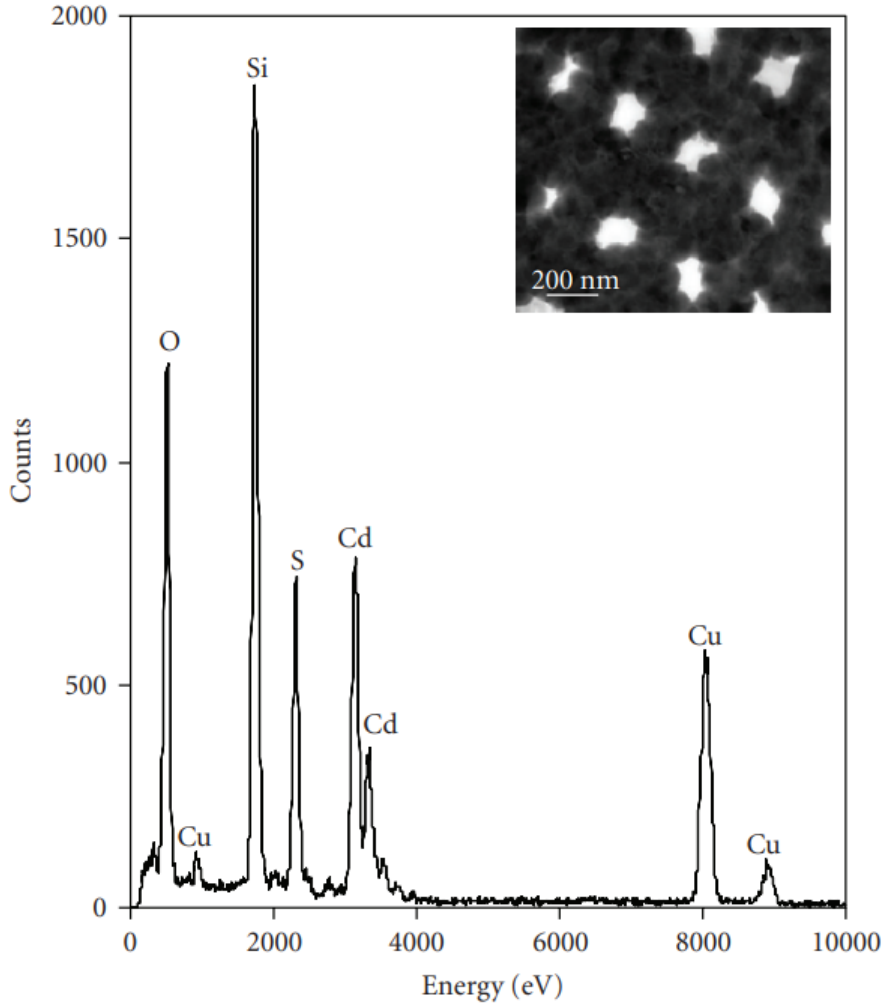

Figure 3.8: TEM micrograph and EDX spectrum details the chemical composition of the CdS-coated diatom frustule shown in the insert. Adapted from Gutu, et al[6].

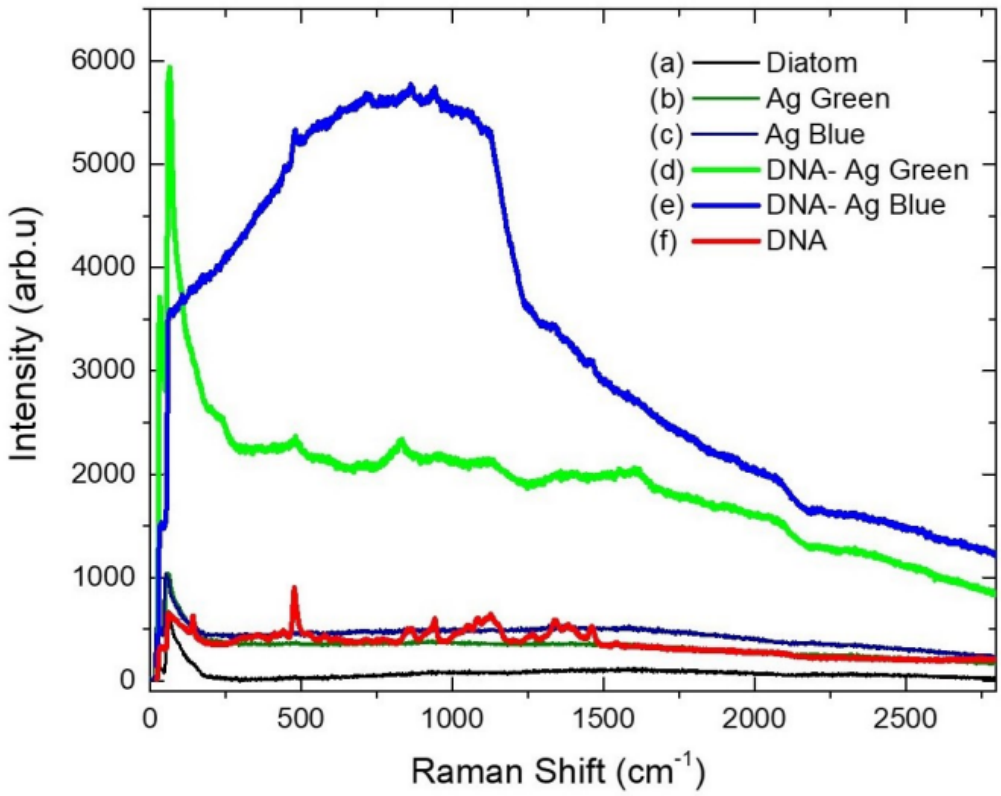

Figure 3.9: Raman spectra of (**a**) diatoms, diatoms irradiated at (**b**) 540 nm (Ag Green), (**c**) 440 nm (Ag Blue). Diatoms with DNA, irradiated at (**d**) 540 nm (DNA Ag Green), (**e**) 440 nm (DNA Ag Blue), and (**f**) DNA pristine, measured with 633 nm excitation wavelength. Adapted from Leon, et al[7].

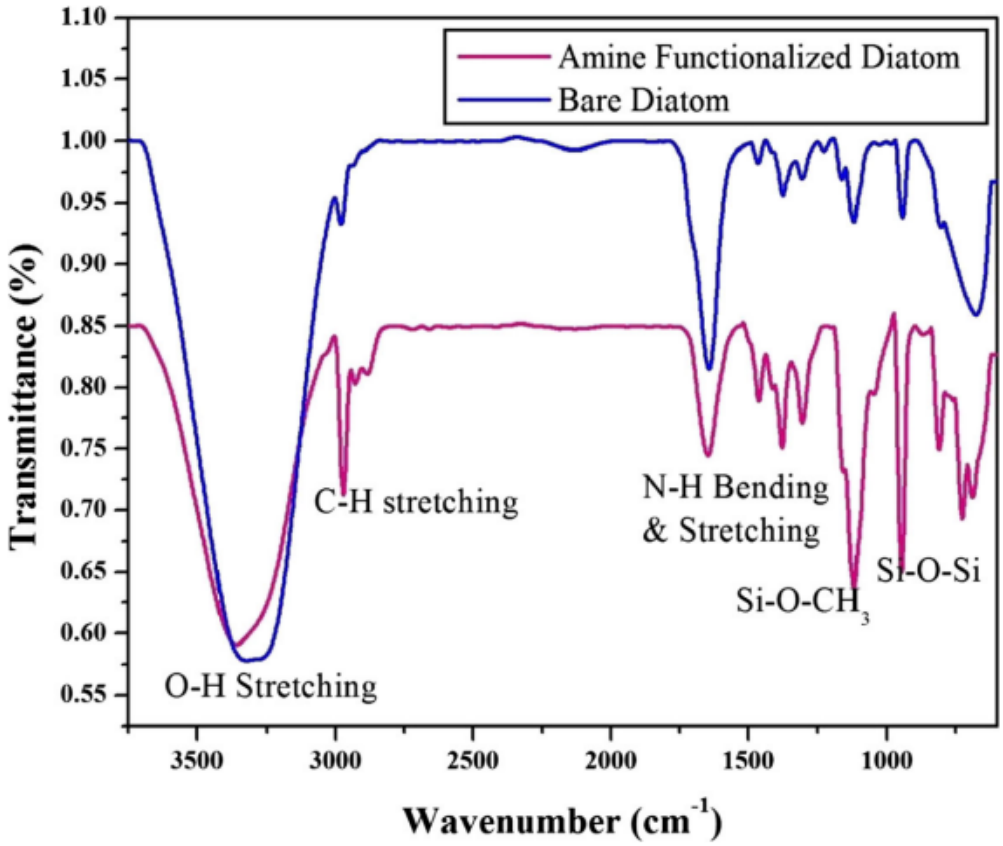

Figure 3.10: FTIR spectra of diatom frustules before and after amine functionalization. Adapted from Viji, et al[8].

analyzed. This allows researchers to assess interactions between the diatom matrix and the nanoparticles and the structural modifications induced by nanoparticle incorporation. FTIR spectra provide insights into chemical bonding and potential surface functionalization of the composite as the example provided in Figure 3.10 retrieved from Viji, et al[8]. This offers valuable information for optimizing synthesis processes and tailoring properties[94,95].

FTIR spectroscopy can be extended to imaging mode, enabling spatially resolved chemical analysis of diatom structures. FTIR imaging generates spectral data at multiple points across a sample, facilitating the creation of chemical maps. FTIR imaging reveals compositional variations within diatom frustules and nanoparticle-doped regions by mapping specific vibrational modes. This technique allows for the visualization of nanoparticle distribution, quantifying chemical constituents, and determining particle-matrix interactions at the microscale. FTIR imaging is essential for comprehensive diatom characterization, enhancing our understanding of hybrid materials for various applications[92,93].

3.9.6 Fluorescence Microscopy

Fluorescence Microscopy is an imaging technique widely employed to visualize and study biological and material samples at the microscopic level. The fundamental principle of fluorescence microscopy involves exciting fluorescent molecules or entities by illuminating them with the light of a specific wavelength. These entities emit fluorescent light at longer wavelengths upon excitation, allowing for their visualization and analysis. Fluorescence microscopy offers high sensitivity, selectivity, and spatial resolution, making it a versatile tool for investigating molecular and cellular processes. The technique provides insights into localization, distribution, and interactions of fluorescently labeled components within samples [96,97].

Fluorescence Microscopy has emerged as a valuable tool for characterizing diatoms doped with nanoparticles for pesticide detection. Diatoms, with their intricate frustule structures, can serve as carriers for nanoparticles functionalized with specific probes or pesticide receptors. By employing fluorescence microscopy, researchers can directly visualize the presence and distribution of nanoparticles within the diatom frustules. Fluorescent labels attached to the nanoparticles enable real-time monitoring of interactions between the diatoms and pesticides. Additionally, fluorescence microscopy can provide information about nanoparticle binding affinity, localization, and aggregation on diatom surfaces. This technique aids in understanding the mechanisms underlying pesticide detection and nanoparticle-diatom interactions [98,99].

Fluorescence Microscopy can be combined with other imaging modalities to comprehensively characterize diatom-nanoparticle hybrids. For instance, integrating fluorescence microscopy with Transmission Electron Microscopy (TEM) or Scanning Electron Microscopy (SEM) allows for correlating the fluorescence signals with high-resolution structural information. This multimodal approach enables researchers to precisely determine the location of nanoparticles within the diatom frustules and their surrounding environment. By employing complementary imaging techniques, a holistic view of the composite material can be obtained, elucidating the complex interactions between diatoms, nanoparticles, and pesticides [96,97].

Chapter 4

Methodology

4.1 Diatom extraction and cleaning

The diatoms studied in this work were extracted from the valley of Guayllabamba, specifically in the Tanda and Puellaro locations in the province of Pichincha, Ecuador. These diatoms, which are part of the Planktonic species, possess a centric morphology. They belong to the *Aulacoseira genus*, which encompasses a wide variety of species. Within the *Aulacoseira genus*, significant variation and sub-classification result in morphological differences influenced by factors like the environment and geographic location[100]. Diatoms with centric frustules exhibiting bilaterally symmetrical construction are uncommon. The frustules can have concentric, radial, or irregular structures and lack a raphe or pseudoraphe. The valve surfaces can be circular, polygonal, elliptical, or occasionally irregular and boat-shaped. *Aulacoseira* demonstrates adaptability to various environments, thriving in large rivers, ponds, and lakes. It is widely distributed in both time and space compared to other freshwater planktonic organisms and can be found in numerous lakes worldwide.[12,43]. To extract the diatom frustules, we carefully separated the light pale varves from the sedimentary rock with a spatula, which is shown in Figure 4.1. In the light pale section of the rock, it is assumed that there is a higher quantity of complete fossilized diatoms, while in the dark section, there are terrigenous or volcanic sediments. After the extraction process, diatoms were prepared to be cleaned by the ionic exchange to remove inorganic oxides such as Al_2O_3, FeO_3, $CaCO_3$, CaO, K_2O, Na_2O, and MgO. Finally, diatoms extracted from the rock were separated by sonication; in a vessel, diatoms were poured in isopropyl alcohol in a ratio of 1 g in 20 mL, and sonicated for 10 minutes, as shown in Figure 4.2.

In this work, we will use a notation to describe the samples as follows: the diatoms without any decoration will be called (D), and diatoms decorated with gold nanoparticles will be called (DAU). Finally, the diatoms decorated with silver nanoparticles will be called (DAG).

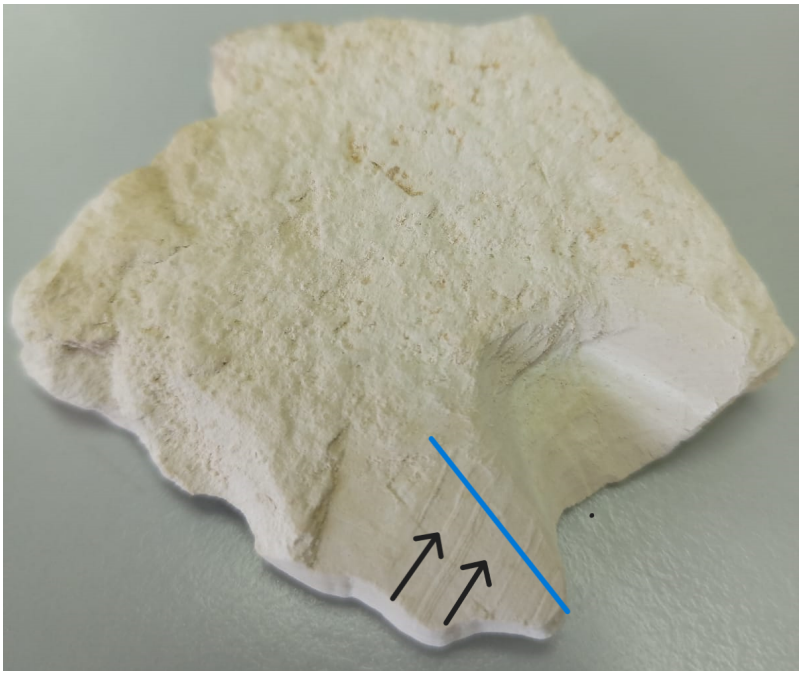

Figure 4.1: Sedimentary rock extracted form Guayllabamba from which diatoms are extracted.

Figure 4.2: Process of sonication of rock source using isopropyl alcohol.

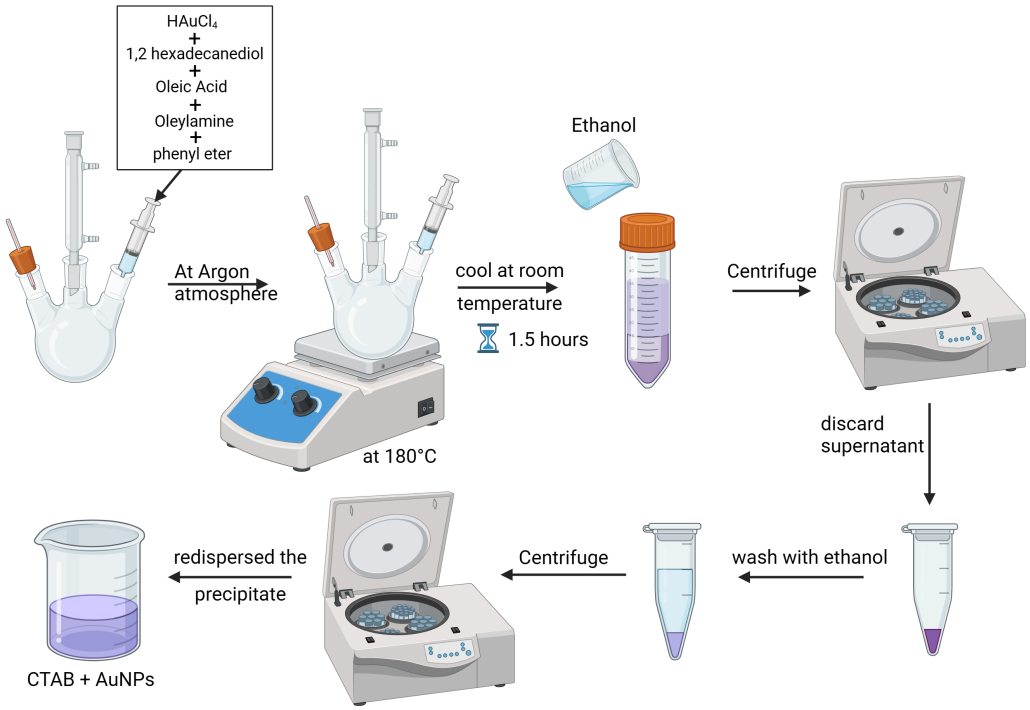

Figure 4.3: Diagram of the process of AuNPs synthesis.

4.2 Synthesis of Gold and Silver Nanoparticles

4.2.1 Synthesis of Gold Nanoparticles

The gold nanoparticles used in this work were previously synthesized using 0.83 g (2.2 mM) of chloroauric acid ($HAuCl_4$), 3.1 g (1.2 mM) of 1,2-hexadecanediol, 0.5 mL (1.5 mM) of oleic acid, and 3 mL (6 mM) of oleylamine were added into 30 mL of phenyl ether. Then, the reaction solution was heated to 180 celsius degrees under an argon atmosphere and vigorous stirring. After that, it was kept at this temperature for 1.5 hours. After cooling to room temperature, ethanol was added to the solution. A dark purple material was precipitated and separated by centrifugation. The precipitated product was washed with ethanol and redispersed in a solution of Cetyltrimethylammonium bromide (CTAB) with a concentration of 0.1 g/100 mL.[101]. A graphical diagram of the synthesis process is shown in Fig.4.3.

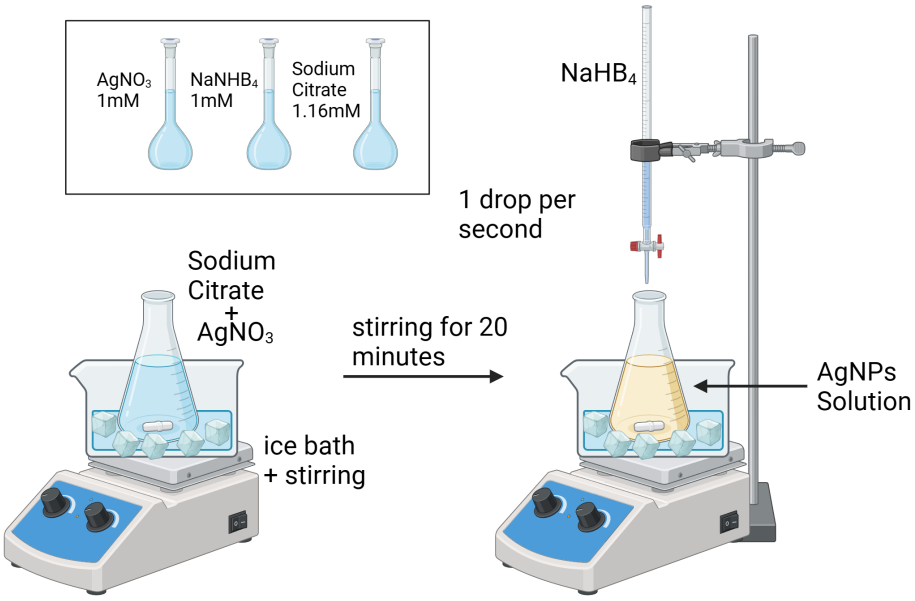

Figure 4.4: Diagram of the process of AgNPs synthesis.

4.2.2 Synthesis of Silver Nanoparticles

Silver nanoparticles were synthesized by reducing silver nitrate ($AgNO_3$) in the presence of Sodium borohydride ($NaBH_4$) and stabilizing them with sodium citrate ($Na_3C_6H_5O_7$). Briefly, an aqueous solution of $NaBH_4$ (1mM) was prepared. 10 mL of 1mM $AgNO_3$ was added with 10 mL of 1.16 mM of sodium citrate. The solution was stirred and cooled for another 20 min. Into the stirred solution at approximately 1 drop per second, the $NaBH_4$ was added (2mL). Stirring the solution was stopped after all of the $NaBH_4$ was added. The graphical diagram of the synthesis process is shown in Fig.4.4 The reaction was allowed to take place until the color changed to a greenish-yellow solution, as shown in Figure.**??**.

4.3 Diatoms decorated with gold and silver nanoparticles

For decorating the diatom frustules with silver and gold nanoparticles, 1 g of diatom powder ground was weighed and placed in 20 mL of ethanol at room temperature. We prepared 4 samples for two different amounts of silver and gold nanoparticles. Then 0.01 g and 0.05 mL of Au/CTAB and Ag NPs were added, respectively (Figure 4.6). Then they were left in the oven for three hours at 60°C. The diagram of the process done in the decoration of diatoms is shown in Fig.4.5

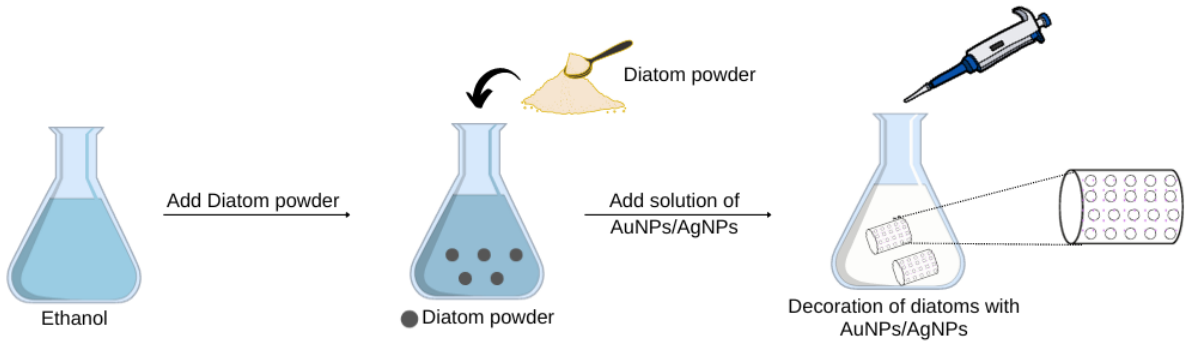

Figure 4.5: Diagram of the process of decoration of diatoms with AgNPs and AuNPs nanoparticles.

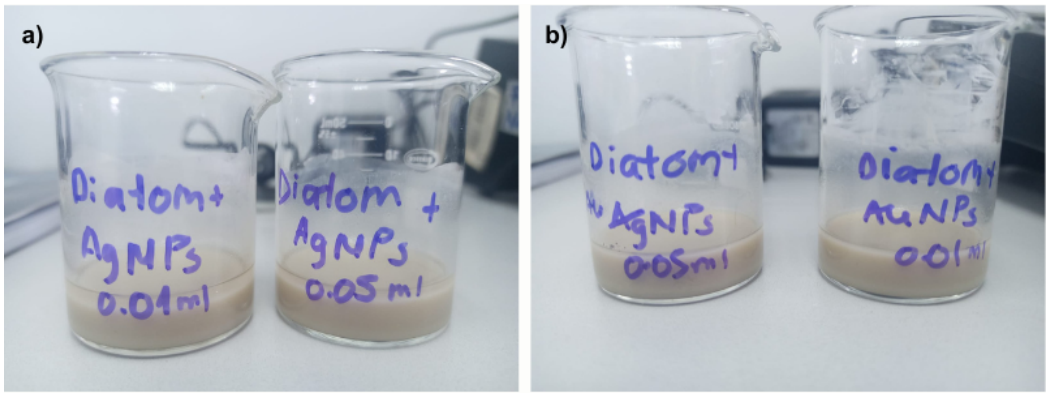

Figure 4.6: **a)** Diatoms doped with 0.01 ml of Ag NPs (left) and 0.05 ml of Ag NPs (right). **b)** Diatoms doped with 0.01 ml of Au/CTAB (left) and 0.05 ml of Au/CTAB (right).

Table 4.1: Diatoms sample codes

Samples Codification	
Type of Sample	Code
Diatom	D
Diatom + 0.01 AuNPs	DAU01
Diatom + 0.05 AuNPs	DAU05
Diatom + 0.01 AgNPs	DAG01
Diatom + 0.05 AgNPs	DAG05

Table 4.2: Diatoms sample codes

Diatoms Codification	
Type of Sample	**Code**
Atrazine	ATR
Diatom	D
Diatom + AuNPs	DAu
Diatom + AgNPs	DAg
AuNPs	Au
AgNPs	Ag
Diatom + ATR	DATR
AuNPs + ATR	ATRAu
AgNPs + ATR	ATRAg
Diatom + AuNPs + ATR	DATRAu
Diatom + AgNPs + ATR	DATRAg

4.3.1 Codes

In Tables 4.1 and 4.2, the codification of the samples is given. These codes will be referred to in the following sections.

4.4 Atrazine adsorption process

The commercial atrazine used in this work is the most used in Ecuador by the distribution of Equaquimica, and the industry is "Syngenta Agro S.A." (Figure 4.7). For this experiment, it is also important to look at all the components of this commercial atrazine to justify the analysis of each technique.In Figure 4.8, the security data of the atrazine from Syngenta S.A.

For the atrazine adsorption experiments, we compared the adsorption behavior of 5 samples: diatoms doped with AuNPs and diatoms doped with AgNPs in each concentration (0.01 mL and 0.05 mL). The experiments were

Figure 4.7: Commercial atrazine of Syngenta.

atrazina (ISO)	1912-24-9	>= 90 -<= 100
lignosulfonic acid, sodium salt	8061-51-6	>= 1 -< 5
sodium dibutylnaphthalenesulphonate	25417-20-3	>= 1 -< 3
gum arabic	9000-01-5	>= 1 -< 5
sodium 2-[methyloleoylamino]ethane-1-sulphonate	137-20-2	>= 1 -< 2,5

Figure 4.8: Commercial atrazine bag components.

done in 10 mL of distilled water with 0.01 g of atrazine, and then 0.01 g of diatom (doped and no-doped) was added (figure 4.10).The diagram in Fig.4.9 The absorbance was measured using the UV-vis spectrometer as a function of the time for several days to calculate the maximum adsorption capacity of the samples.

4.5 Kinetic Adsorption Analysis

The kinetics describe the rate of adsorption of commercial atrazine in the surface of the diatoms and decorated diatoms. This determines the time in which the equilibrium is reached. The adsorption capacity Q_t (mg/g) and removal rate R (%) were used as the parameters that reflect the performance of the adsorbent. Equation for calculate

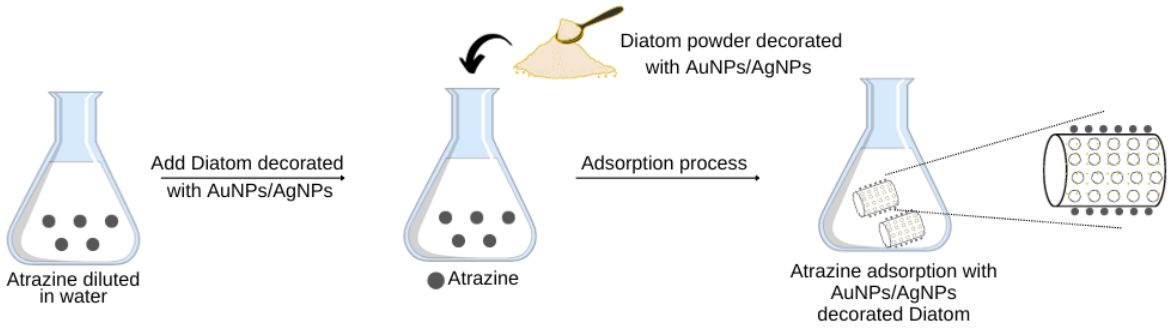

Figure 4.9: Diagram of the atrazine adsorption process

Figure 4.10: Atrazine with the diatom samples in the adsorption process.

Q_t and R are the following:

$$Q_t = (C_0 - C_t).\frac{V}{m} \tag{4.1}$$

$$R = (C_0 - C_t)/C_0.100\% \tag{4.2}$$

where, C_0 is the initial concentration of atrazine, C_t is the concentration of atrazine in mg/L at time t in min, V is the volume of the solution in L and m is the mass of diatoms in g.

The adsorption process of commercial atrazine on diatoms and diatoms decorated with silver and gold nanoparticles at different concentrations were simulated by the pseudo-first-order kinetic model and pseudo-second order kinetic. Different models can be expressed by the following equations:

Pseudo-first order kinetic equation (PF0)

where Q_t is the adsorption capacity (mg/g), Q_e is the equilibrium adsorption capacity (mg/g); t is the time (min) and k_1 = rate constant (min^{-1}).

$$ln(Q_e - Q_t) = lnQ_t - k_1 t \tag{4.3}$$

where Q_t is the adsorption capacity (mg/g), Q_e is the equilibrium adsorption capacity (mg/g); t is the time (min) and k_1 = rate constant (min^{-1}).

Pseudo-second order kinetic equation (PSO)

$$\frac{t}{Q_t} = \frac{1}{k_2.Q_e^2} + \frac{t}{Q_e} \tag{4.4}$$

where k_2 is the pseudo-second-order rate constant. The other labeled variables and constants have the same meanings as in the PFO model. Plotting t/Qt vs t gives a straight line for PSO- compliant kinetics. The slope of the linear plot give us k_2. Furthermore, in environmental studies focusing on adsorption kinetics, the Pseudo-First-Order (PFO) and Pseudo-Second-Order (PSO) models take precedence as the most frequently employed models. They serve as valuable tools for discerning whether the adsorption process is primarily of a physical or chemical nature. If the pseudo-first-order model yields a superior fit, it means a physical adsorption process, whereas a superior fit of the pseudo-second-order model indicates chemical adsorption[74,77].

4.6 Characterization

4.6.1 UV-Vis spectroscopy

The UV-vis spectra of AuNPs, AgNPs, solution of atrazine, diatoms decorated with AuNPs and diatoms decorated with AgNPs were taken with an Ultraviolet-Visible spectrometer JENWAY Genova Nano (Figure 4.11).

4.6.2 Raman spectroscopy

The Raman spectra were taken with a Raman spectrometer HORIBA LabRAM HR Evolution (Figure 4.12) using a laser of 533 nm.

The sample preparation to analyze using the Raman spectrometer was done in different glass slides and let dry in order to put them in the optical microscope adapted from the Raman spectrometer using a laser of 533 nm (Figure 4.13).

4.6.3 Scanning Electron Microscopy (SEM) and Energy Dispersive X-ray microanalysis (EDS)

The scanning electron microscopes used were the TESCAN MIRA 3 Schottky field scanning electron microscope, working with an acceleration voltage of 10 KV attached with an energy dispersive X-ray microanalysis (EDS Bruker

Figure 4.11: UV-vis spectrometer JENWAY Genova Nano.

Quantax), and the PHENOM PRO X, with software pro suite detector fast SDD from AMPTEK (Figure 4.14). EDX was measured using the EDS Bruker Quantax. For the sample preparation, a minimum quantity of dry powder of each sample was used in a piece of carbon specialized for this type of equipment and placed in a metal tip. Both of them belongs to ESPE University

4.6.4 Fluorescence microscopy

The Fluorescence microscope used was the Olympus BX63 optical microscope with a fluorescence device (Figure 4.15).

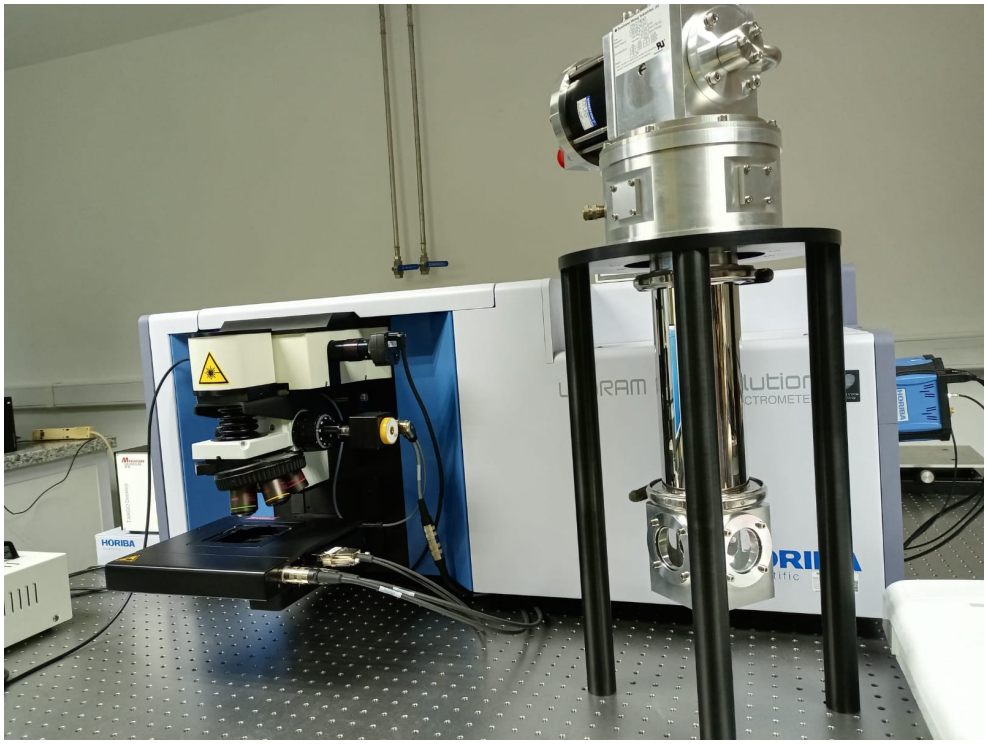

Figure 4.12: Raman spectrometer, HORIBA LabRAM HR Evolution.

4.6.5 Fourier Transform Infrared spectrometer (FTIR)

The Fourier Transform Infrared spectrometer used was the Agilent Cary 630 FTIR spectrometer (Figure 4.16).

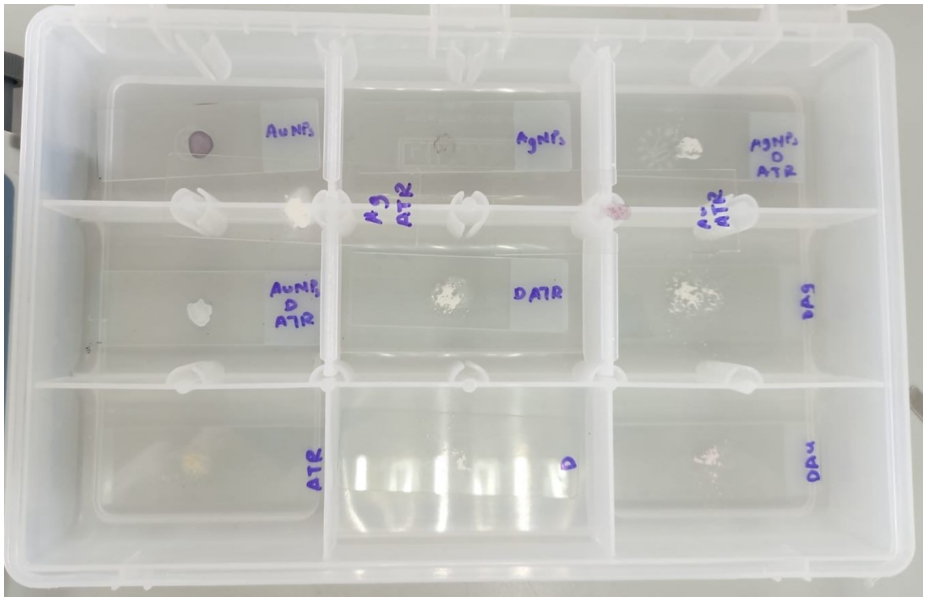

Figure 4.13: Sample preparation for Raman spectrometer and Fluorescence microscope.

Figure 4.14: Scanning electron microscope PHENOM PRO X.

Figure 4.15: Olympus BX63 optical microscope.

Figure 4.16: Fourier Transform Infrared spectrometer.

Chapter 5

Results & Discussion

5.1 UV Vis spectroscopy

In order to characterize the nanoparticles synthesized previously and the components used in the experimentation, such as atrazine and diatoms, as well as the decorated ones. It is performed in the UV vis spectrometer of each one of the samples (Figure 5.1). In this figure, it can be observed the UV-vis spectra of each material used in this work.

As it is observed in the black line, the peak at 404 nm corresponds to the characteristic absorption of silver nanoparticles [102], and as it can be seen in Figure 5.2, the yellowish color of the aqueous solution, it is a qualitative indication of the formation of the nanoparticles [103]. In the yellow line, the absorbance peak at 525 nm corresponds to the formation of gold nanoparticles [104], and in Figure 5.2, we observe the red-purple aqueous solution characteristic of the gold nanoparticles [104]. The purple line corresponds to the diatom sample; there is no signal that we can determine from it as well as the blue and green lines in which the signal is the same because those correspond to the diatom decorated with silver and gold nanoparticles. Diatoms overlap the signal of the nanoparticles, which is why it cannot be observed those peaks characteristic of each type of nanoparticle; in the following section, it is used SEM and EDX to confirm the presence of those nanoparticles on the surface of the diatoms. Finally, in the red line, a peak around 228 nm corresponds to the atrazine sample [105].

5.2 Scanning Electron Microscopy (SEM).

This section described the scanning electron microscopy characterization of the diatoms decorated with silver and gold nanoparticles respectively. This technique was used to observe the morphological characteristics of the diatoms, such as the diameter of the pores, the presence of nanoparticles, and their distribution on the diatom's surface. The determination of the diatom size and pore size was made using the ImageJ software.

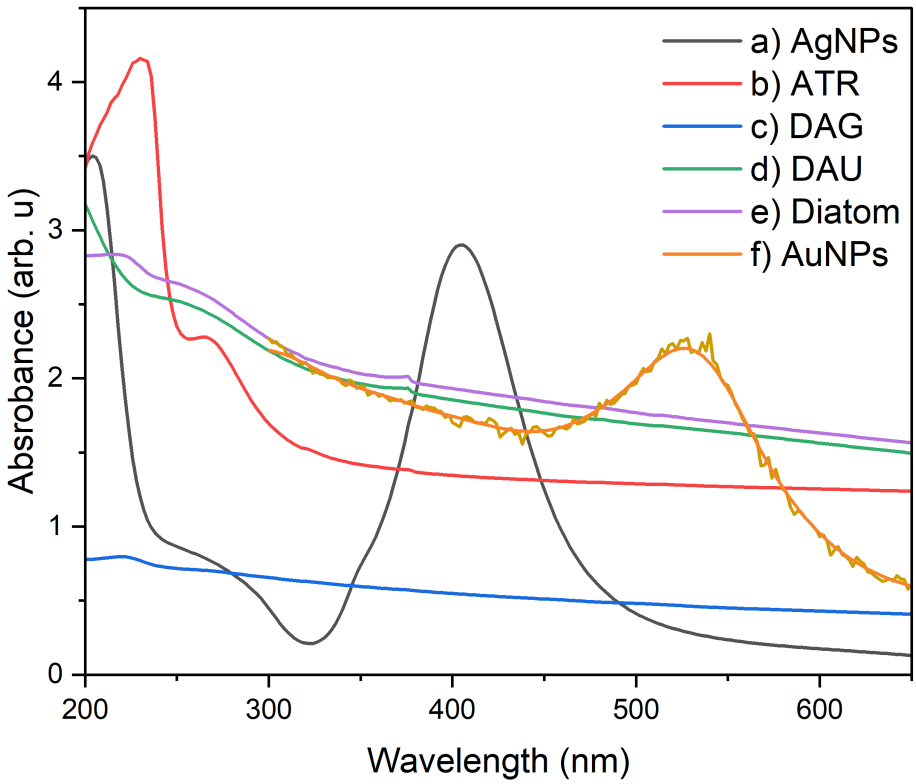

Figure 5.1: UV-vis spectrum of **(a)** Silver Nanoparticles (AgNPs), **(b)** Atrazine (ATR), **(c)** Diatoms decorated with Silver Nanoparticles (DAG), **(d)** Diatoms decorated with Gold Nanoparticles (DAU), **(e)** Diatoms, **(f)** Gold Nanoparticles (AuNPs).

Figure 5.3 shows the micrograph of the cleaned diatom without any decoration of nanoparticles (D). It can be seen in its average diameter of 6.35 μm and the average length of the cylindrical diatom of 20.76 μm. Moreover, the whole structure and porosity of the diatom can be observed, and in the surroundings of that complete structure, it is also observed some other broken structures with similar characteristics. Using ImageJ software, it was determined the average particle size of the pores of 500 nm. Figure 5.3 shows the histogram of the pore size of the diatom observed in the micrograph. Most of the pores were in the average size mentioned on that side of the diatom structure. From this micrograph, it is determined the type of diatom used, according to Zamora, J in comparison with the dimensions, and the structure described corresponds to *Aulacoseira genus* [106].

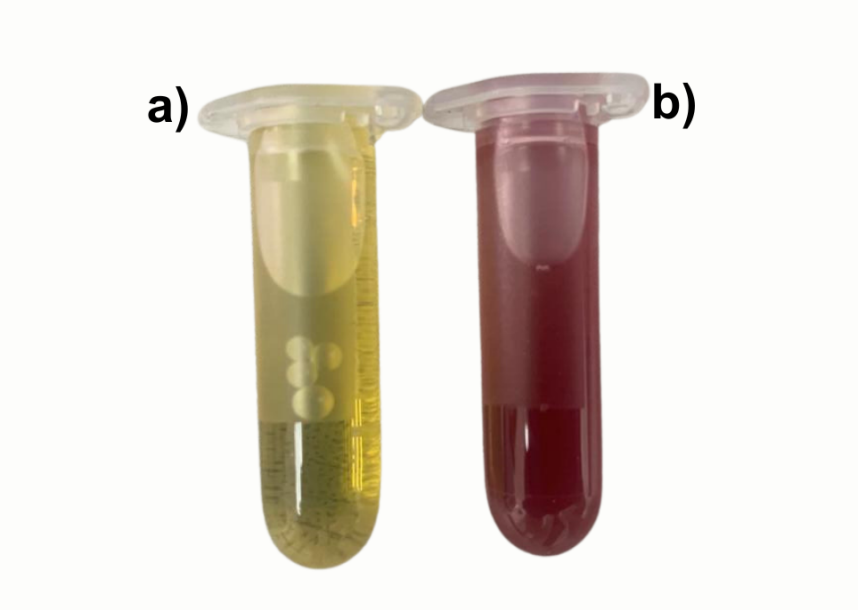

Figure 5.2: **(a)** Silver nanoparticles (yellow solution) and **(b)** Gold nanoparticles (red-purple solution).

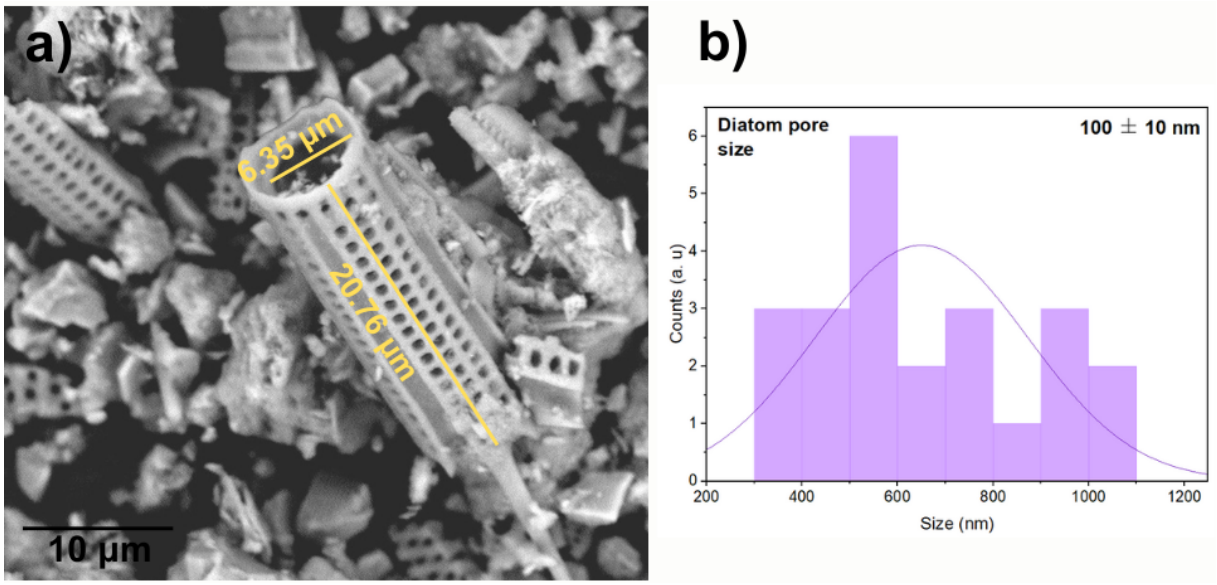

Figure 5.3: SEM micrograph of **(a)** Diatoms and **(b)** pore size distribution.

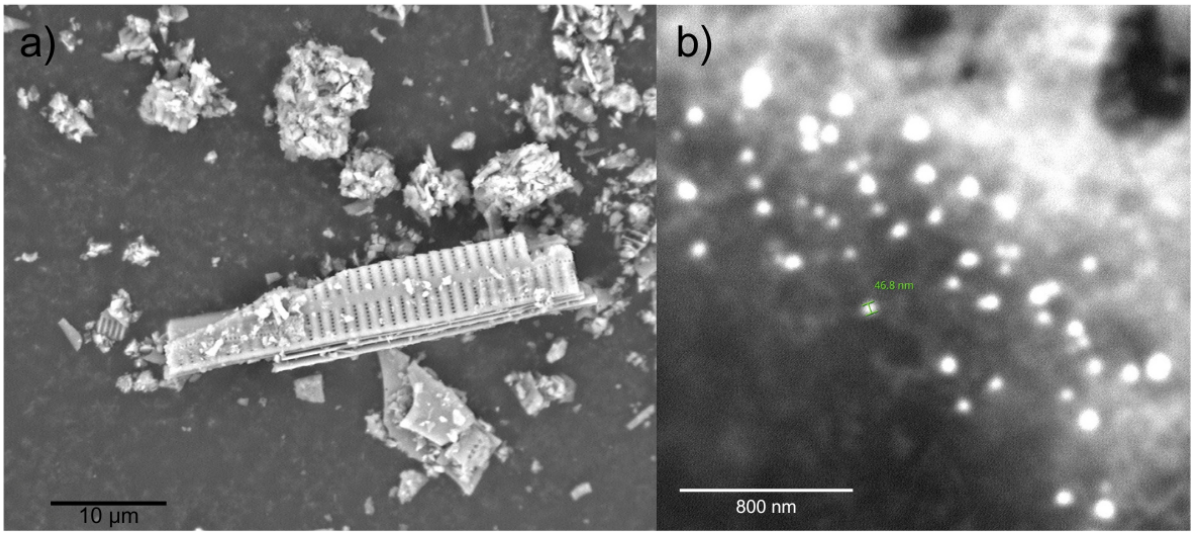

Figure 5.4: SEM micrograph of Diatoms decorated with silver nanoparticles (DAg). **a)** large perspective of the sample (10 μm scale) and **b)** closer look of the sample 800 nm.

Figure 5.4 shows the micrographs of the diatoms decorated with silver nanoparticles (DAg). As can be seen, the sample presents a broken structure, and the AgNPs appear as brighter dots in comparison with the diatom structure due to the difference in atomic number. Figure 5.4 (b) shows a closer look of the diatoms decorated with silver nanoparticles, showing the diameter of one of them in the brighter dots with a size of 46.8 nm. This confirms the decoration of the surface of the diatom with silver nanoparticles.

Figure 5.5 shows the diatoms decorated with gold nanoparticles. Figure 5.5 a) shows some complete and broken diatom structures and Figure 5.5 b) is a magnified image of Figure 5.5 a) the area magnified is highlighted by a yellow square. From this Figure, a broken structure of the diatom decorated with AuNPs it is observed in the brighter areas of the micrograph. To complement the analysis in the following section, the samples will be analyzed with EDX.

5.3 Energy Dispersive X-Ray spectroscopy (EDX)

The Elemental mapping analysis of the Diatoms decorated with AuNPs was measured using energy-dispersive X-ray spectroscopy. Figure 5.5 shows the homogeneous distribution of Si, Na, and Au elements on the diatom surface, confirming the effective decoration with the gold nanoparticles.

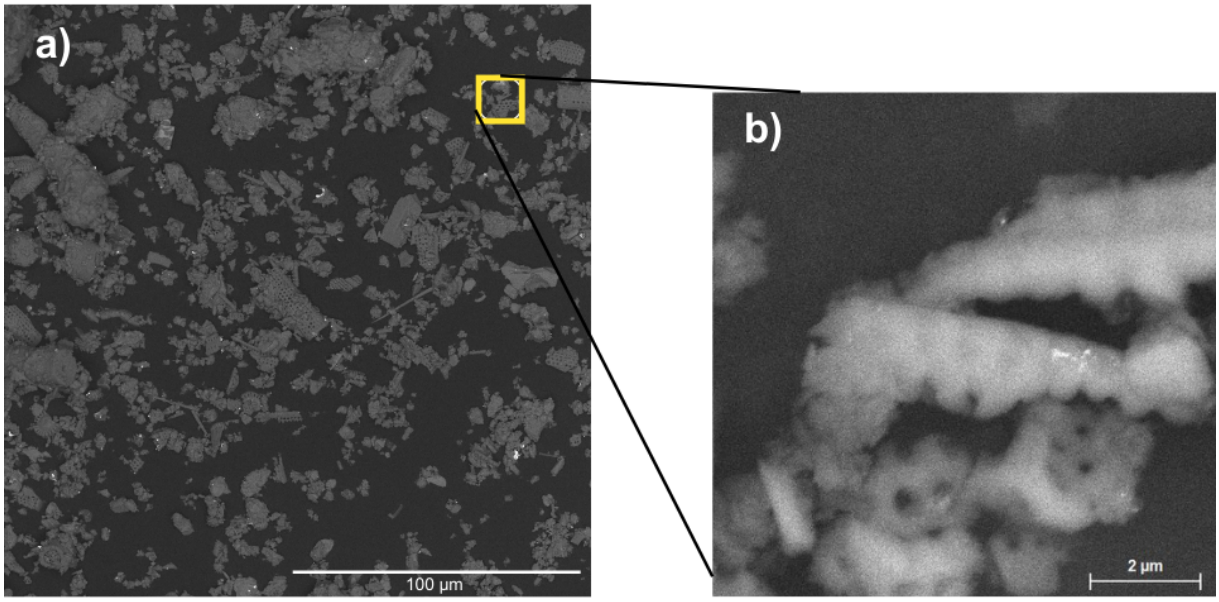

Figure 5.5: SEM micrograph of Diatoms decorated with gold nanoparticles (DAu). **a)** General view showing complete frustules and broken ones and **b)** of-inset in image a).

Figure 5.5 shows the elements present in the sample. As it can be appreciated, each color, particularly the purple and red ones, of silicon (b) and oxygen (d), respectively, represents the diatom frustule skeleton [107]. Moreover, the Figure 5.5 (f) one demonstrates the presence of gold nanoparticles in the diatom surface. It is important to mention that in Figure 5.5 (a) is observed, confirming the distribution of the AuNPs on the surface of the diatom skeleton.

Table 5.1 is a summary of the weight percentage of each element present in the area analyzed by EDX plot from Figure 5.7 in which it is determined the quantity of the elements shown in Figure 5.6. The percentage of each is expected as it confirms the presence of silicon oxide SiO_2 because it is the principal material of the diatom [107]. The higher percentage of silicon and oxygen, respectively, confirms it. Moreover, the presence of gold is also confirmed in a considerable percentage of 1.2%. It is also important to remind about the other element and that these may come from the leftovers; even after the cleaning process has been done to eliminate these impurities, some remains.

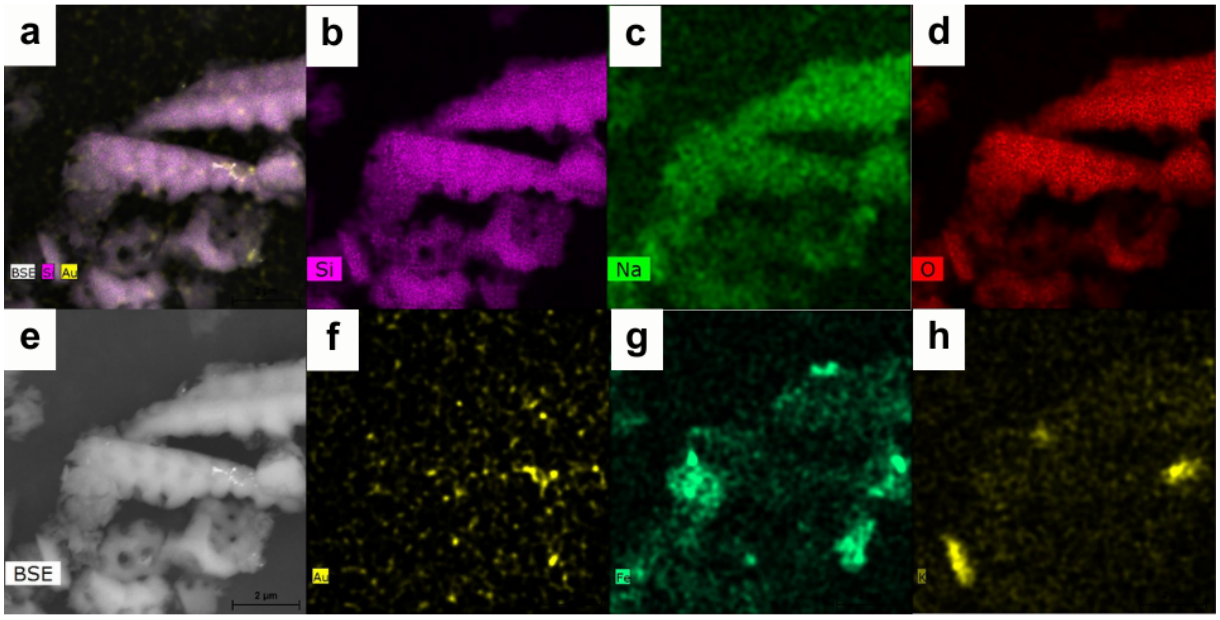

Figure 5.6: Elemental Mapping Analysis of Diatoms decorated with AuNPs.

Table 5.1: EDX analysis, present elements in the area (yellow square) showed in Figure 5.5.

Area of diatoms decorated with gold nanoparticles (DAu)			
Atomic number	**Element Symbol**	**Element name**	**Atomic Concentration (%)**
8	O	Oxygen	65,4
11	Na	Sodium	1,91
12	Mg	Magnesium	0,87
13	Al	Aluminum	2,52
14	Si	Silicon	26,5
19	K	Potasium	0,17
20	Ca	Calcium	0,29
26	Fe	Iron	1,13
79	Au	Gold	1,2

5.4 Fourier Transform Infrared spectroscopy (FTIR)

The FTIR analysis was done in the 4000-450 cm^{-1} range. The results are shown in Figure 5.8 for a) diatoms, AuNPs, atrazine (ATR), atrazine with diatoms (DATR), atrazine with AuNPs (ATRAu), and atrazine combined with diatoms

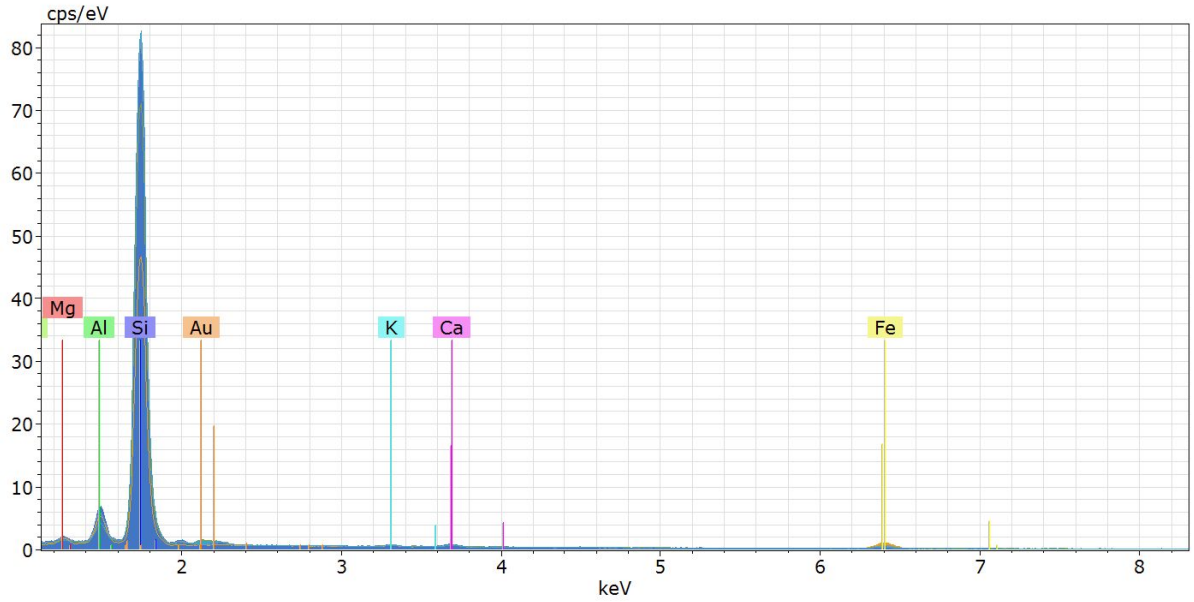

Figure 5.7: EDX Analysis of Diatoms decorated with AuNPs.

decorated with AuNPs (DATRAu); and b) diatoms, AgNPs, atrazine (ATR), atrazine with diatoms (DATR), atrazine with AgNPs (ATRAg), and atrazine combined with diatoms decorated with AgNPs (DATRAg).

In Figure 5.8 A), the main vibrations of the diatom (f) are observed at 1035 cm^{-1} assigned to the siloxane (Si-O-Si) stretching, at 792 cm^{-1} from the silanol groups (Si-O), and at 452 cm^{-1} corresponds to the bending vibration of siloxane [108]. These vibrations are characteristic of the silicon dioxide of the diatom structure.

In Figure 5.8 A) and B) in the spectrum e) the bands at 3252 cm^{-1} and 2971 cm^{-1} correspond to N-H and C-H vibrations of atrazine (e) respectively, the bands at 1541 cm^{-1} and 1401 cm^{-1} corresponds to the triazine group and the semicircle ring respectively, the bands at 1167 cm^{-1} and 1056 cm^{-1} are assigned to C-N vibration and triazine ring sextant, and the band at 730 cm^{-1} is assigned to the C-H stretching of aromatic rings [109]. Those values previously described for diatom and atrazine are also listed in Table 5.3 and Table 5.2.

In Figure 5.8 A) and B), the FTIR spectra of the interaction between the diatoms with atrazine (d) are plotted. In this spectra (d), the band between 3381 cm^{-1} and 3227 cm^{-1} is assigned to O-H symmetric and asymmetric stretching as well as the band at 1650 cm^{-1} that is assigned to H-O-H bending, those bands are characteristic from water [110]. Between 1550 cm^{-1} and 992 cm^{-1}, the characteristic peaks previously described from atrazine are present at a lower intensity, showing an interaction between the atrazine and the diatom through the siloxane and silane groups of the diatoms and the N-H groups of the atrazine.

In Figure 5.8 part A), it is represented in the a), b), and c) spectra the samples containing gold nanoparticles

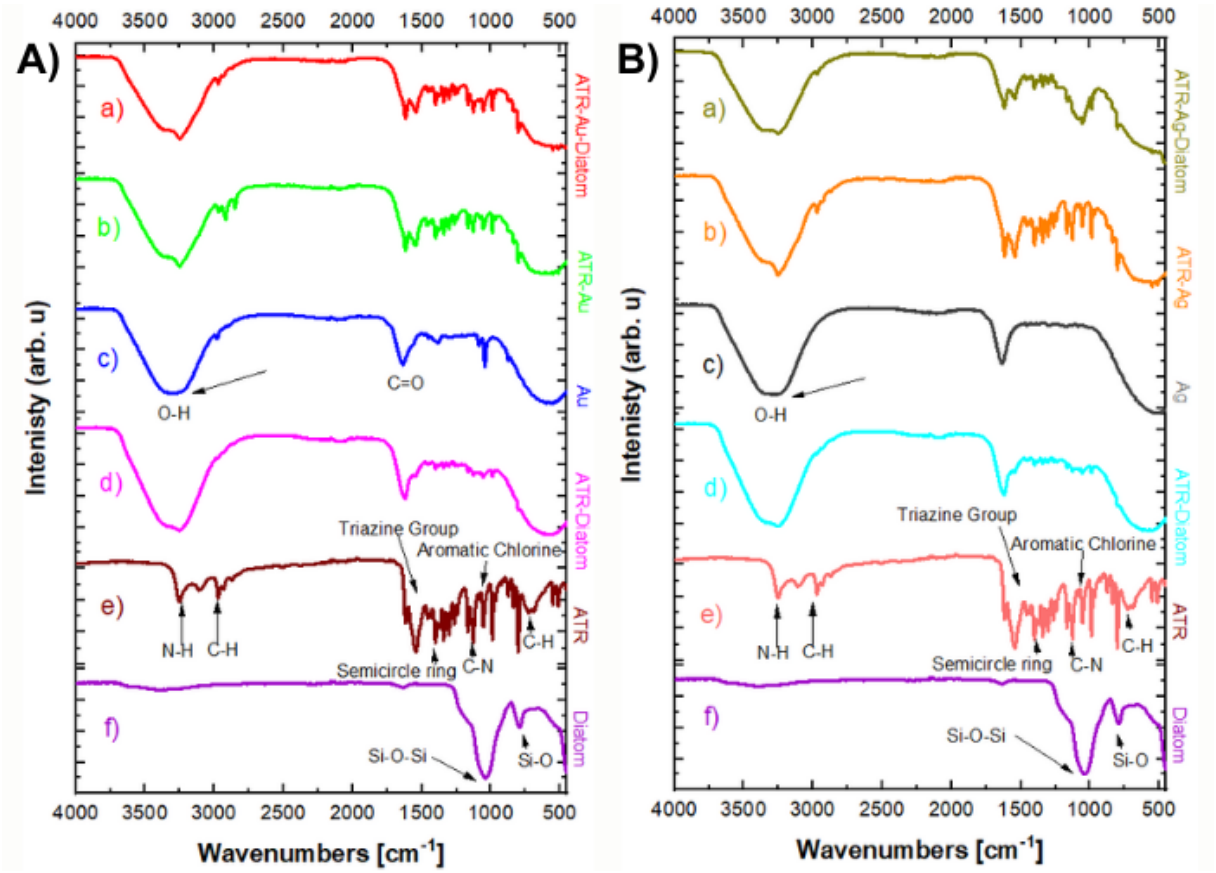

Figure 5.8: Fourier transform infrared spectra of **A**: **(a)** Diatoms decorated with AuNPs + atrazine, **(b)** AuNPs + atrazine, **(c)** AuNPs, **(d)** Diatoms + atrazine, **(e)** Atrazine, **(f)** Diatoms; and **B**: **(a)** Diatoms decorated with AgNPs + atrazine, **(b)** AgNPs + atrazine, **(c)** AgNPs, **(d)** Diatoms + atrazine, **(e)** Atrazine, **(f)** Diatoms.

(Au, ATRAu, and DATRAu). In Table 5.2 are the respective values of each band that appears in those samples evidencing the interaction between those. All the samples in this comparison are in an aqueous solution which is why some of the bands correspond to the ones of water, such as O-H symmetric and asymmetric stretching, and H-O-H bending [110]. The gold nanoparticles spectrum (c) shows a band at 1389 cm^{-1} assigned to C–H stretching vibration. On the other hand, the band at 1644 cm^{-1} (C=O symmetric stretching) due to the CTAB-capped AuNPs [104]. In Figure 5.8 part A, in the spectrum b) and a) is the spectrum of sample ATRAu corresponding to the interaction between gold nanoparticles with atrazine, and the sample DATRAu corresponds to the diatoms decorated with AuNPs with atrazine. In b) spectrum, it is appreciated some characteristic peaks coming from atrazine in the range from 3247 cm^{-1} to 2854 cm^{-1} such as N-H and C-H vibrations showing the interaction of those functional groups with gold nanoparticles. Moreover, those bands from 1544 cm^{-1} to 797 cm^{-1} show the characteristic peaks of atrazine, such

Table 5.2: FT-IR absorption bands for atrazine, diatom, diatoms decorated with AuNPs and their interactions with atrazine.

Assignment	**ATR** (cm^{-1})	**D** (cm^{-1})	**DATR** (cm^{-1})	**Au** (cm^{-1})	**ATRAu** (cm^{-1})	**DATRAu** (cm^{-1})
N-H	3247					
O-H			3316 - 3380	3316 - 3380	3316 - 3261	3316 - 3261
C-N double bonding			1630		1617	1617
C-H stretching	2964			2985	2844	2844
C-H bending				1633 - 1385		
Triazine group	1549		1566		1540	1540
Semicircle ring	1394				1398	1398
C-N bonds	1124				1140	1140
C-O				1051		
Aromatic chlorine	1050				1063	1063
Triazine ring sextant	803					
C-H stretching of aromatic rings	730				793	793
Si-O-Si		1041				
Si-O		790				

as triazine group, semicircle ring, C-N, and aromatic chlorine. These interactions could be attributed to the CTAB capping agent that covers the gold nanoparticle, and then the positively charged amino groups on atrazine may interact with the negatively charged surface of CTAB-capped gold nanoparticles[111]. Furthermore, the spectrum b), was found similarities to the spectra a) of DATRAu in the peaks related to atrazine. The difference between those samples is the bands at 2977 cm^{-1}, which fits with the band of C-H stretching of the atrazine shown in Table 5.2. Another difference from the spectra b) is with the bands between 1128 cm^{-1} and 1050 cm^{-1} assigned to the characteristic peaks of atrazine that comes from C-N and aromatic chlorine[109] shown in Table 5.2, the intensity of those increase in comparison with the spectrum b) of ATRAu and d) DATR, showing an increasing of the molecules of that type interacting with the sample, showing a potential enhance in the adsorption of atrazine with the diatoms decorated with gold nanoparticles in comparison with diatoms, and gold nanoparticles separated.

In Figure 5.8 part B) it is represented in the c), b), and a) FTIR spectrum of the sample containing silver nanoparticles (Ag, ATRAg, and DATRAg). In Table 5.3 are the respective values of each sample. In the spectrum c) of silver nanoparticles in an aqueous solution were synthesized using $NaHB_4$ as the reducing agent and sodium citrate as the stabilizing agent. The band at 1638 cm^1 is associated with COO- stretching vibration that comes from the citrate capping[112] of the silver nanoparticles that acts as a stabilizer in the formation of those nanoparticles. In the case of the b) FTIR spectrum of the sample ATRAg clearly marks the presence at 1405 and 1528 cm^{-1}; of the

Table 5.3: FTIR absorption bands for atrazine, diatom, diatoms decorated with AgNPs and their interactions with atrazine.

Assignment	**ATR** (cm^{-1})	**D** (cm^{-1})	**DATR** (cm^{-1})	**Ag** (cm^{-1})	**ATRAg** (cm^{-1})	**DATRAg** (cm^{-1})
N-H	3247					
O-H			3316 - 3380	3395 - 3212	3316 - 3261	3386 - 3206
C-N double bonding			1630		1617	
-Br stretching				586 - 470		
CONH2				1638		1619
C-H stretching	2964				2844	
C-H bending						
Triazine group	1549		1566		1540	1542
Semicircle ring	1394				1398	1387
C-N bonds	1124				1140	
C-O						
Aromatic chlorine	1050				1063	1066
Triazine ring sextant	803					809
C-H stretching of aromatic rings	730				793	
Si-O-Si		1041				
Si-O		790				

symmetric and antisymmetric stretching vibrations of COO-, respectively[113]. Since some other bands in this b) FTIR spectrum of ATRAg, such as the one corresponding to C-N stretching, aromatic chlorine and C-H are observed as it follows in Table 5.3 showing an interaction between atrazine and silver nanoparticles citrate-capped. Moreover, with the FTIR spectrum a) of sample DATRAg, there are some differences in some of the interactions between the functional groups of atrazine and the diatoms decorated with silver nanoparticles. In comparison from a) spectrum of sample DATRAu of Figure 5.8 part A), it is a difference between the vibration bands in 1157 cm^{-1}, 1050 cm^{-1}, and 982 cm^{-1} that are assigned to C-N stretching, aromatic chlorine and C-H vibration respectively that corresponds to the ones of atrazine showing a interaction between the sample of diatoms decorated with silver nanoparticles and those functional groups. In particular, the band assigned to aromatic chlorine increases in comparison with the sample of DATRAu, showing the increasing concentration of that molecule, interacting more with diatoms with silver nanoparticles than diatoms with gold nanoparticles.

5.5 Raman spectroscopy

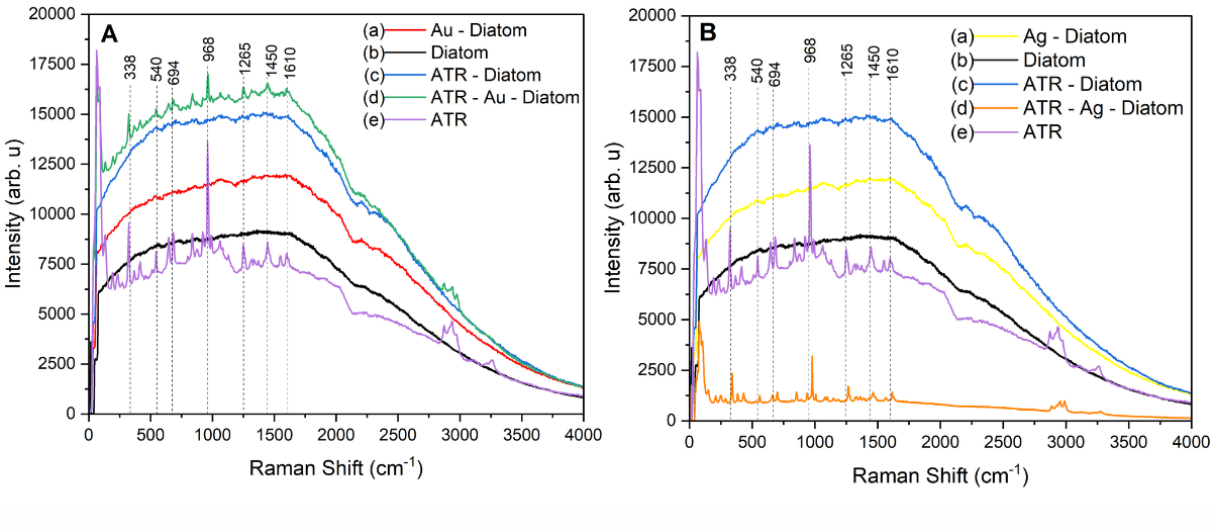

Figure 5.9: Comparison between Raman spectra for **A** AuNPs interactions and **B** AgNPs interactions.

Figure 5.9 shows the Raman spectra of atrazine and the comparison between the samples to denote it. Figure 5.9 a) shows the comparison within the samples using the diatoms doped with gold nanoparticles, and Figure 5.9 b) the comparison within the samples using diatoms doped with silver nanoparticles. In order to determine the characteristic peaks of atrazine in both samples, it is important to assign the vibration bands to each of them. The Raman spectra of atrazine show the principal bands at 540 cm^{-1} is assigned to Cl-Cl stretching, at 694 cm^{-1} is assigned to C-C symmetric stretching, at 843 cm^{-1} is assigned to CO_3 asymmetric bending vibration and at 968 cm^{-1} is assigned to C-H out of plane deformation vibration [114]. Moreover, the other bands reported are in good agreement with Costa, et al. The band at 1265 cm^{-1} is assigned to ring mode 14 and N-H bending, the band at 1450 cm^{-1} is assigned to CH_2 and CH_2 bending; and the band at 1610 cm^{-1} is assigned to N-H bending and C-N stretching [115].

To understand deeply the interactions from decorated diatoms and atrazine as well as the differences from using diatoms decorated with AgNPs from the ones decorated with AuNPs, the Figure 5.9 is analyzed. It is important to remark that in Figure 5.9.A and 5.9.B there are plotted in both of them the Raman spectra of Diatoms (b), atrazine (ATR) (e), and atrazine with diatoms (ATR-Diatom) (c). It is observed that diatoms themselves are fluorescent due to amorphous silica in its structure. diatoms showed a broad-band in the range 300–3000 cm^{-1}, which was attributed to the fluorescence due to Qx and Qy electronic modes [116]. Moreover, diatoms have unique properties that enable them to exhibit photon crystal-like behavior. These type of frustules have highly ordered, periodic nanostrucuture

from which the photonic crystal like behavior comes from. Due to this periodicity and the difference of refractive indices (silica and air) it causes selective scattering and diffraction of light.[117,118]. On the other hand, the Raman spectra of diatoms decorated with AuNPs (Au-Diatom) and of diatoms decorated with AgNPs (Ag-Diatom) enhance the Raman signal of the diatoms. In agreement with Briceno, et al the fluorescence at 633 nm excitation wavelength of the diatoms decorated with gold nanoparticles confirm the behaviour of the electronic modes with the increasing of fluorescence intensity in diatoms[101] and with AgNPs occurs similar. This phenomena comes from silver and gold nanoparticles and their localized Surface Plasmon Resonance (LSPR). These LSPR-induced electromagnetic fields near the surface of AgNPs and AuNPs are much stronger than the incident electromagnetic field, and this results in an enhancement of local electric field strength leading to the enhancement interactions with the molecules for which are adsorbed or closed them[114,118].

Since it was analyzed the interaction within diatoms and nanoparticles (Ag and Au), now how these decorated diatoms behaves in the adsorption of atrazine. First, for Figure 5.9.A, the Raman spectra of atrazine with diatoms decorated with gold nanoparticles it appears a increase of intensity of the signal in comparison with the sample of diatoms decorated with AuNPs (a), and at the same time the characteristic peaks of atrazine previously described are clearly observed. From this, diatoms decorated with AuNPs enhance the signal of atrazine not only form the photonic crystal behaviour of diatoms but also from the localized surface plasmon resonance that comes from the gold nanoparticles. However, it does not occurs the same effect with diatoms decorated with silver nanoparticles (a) from Figure 5.9.B. In this spectra it is observed a decreasing of the atrazine Raman characteristic peaks and the brand that comes from diatoms it is not observed. This could be attributed to the fact that the difference of size between AuNPs and AgNPs is considerably big, and from a better localized surface plasmon resonance it is dependant from the size of nanoparticles and in this case for AuNPs in an average size of 10nm it has a better LSPR which is useful in the enhancement of atrazine Raman signal.

5.6 Fluorescence Microscopy

For fluorescence microscopy, with an excitation wavelength of 470 nm the samples were irradiated. Using this characterization technique, it was possible to identify and correlate the fluorescence of the samples of diatoms doped with nanoparticles and the enhancement of this fluorescence for atrazine detection. This fluorescence is due to the intrinsic optical properties of the diatoms that come from its photonic crystal-like behavior and the surface plasmon resonance of the nanoparticles enhancing the signal of atrazine. Figure 5.10 and Figure 5.11 are the comparison images of fluorescence microscopy corresponding to the ones with silver nanoparticles and gold nanoparticles, respectively. In Figure 5.10-A and 5.11-A, the diatoms frustules are presented, and as it was mentioned before, they are fluorescent themselves, and their emission is observed at 470 nm in agreement with Leon, et al results[119]. Then, for the sample of diatoms with atrazine (Figure 5.10-C and 5.11-C), there are no significant changes in the fluorescence from the one with one only with diatoms.

Figure 5.10 also presented the fluorescence microscopy of AgNPs (D) showing brilliant dots, then the one with

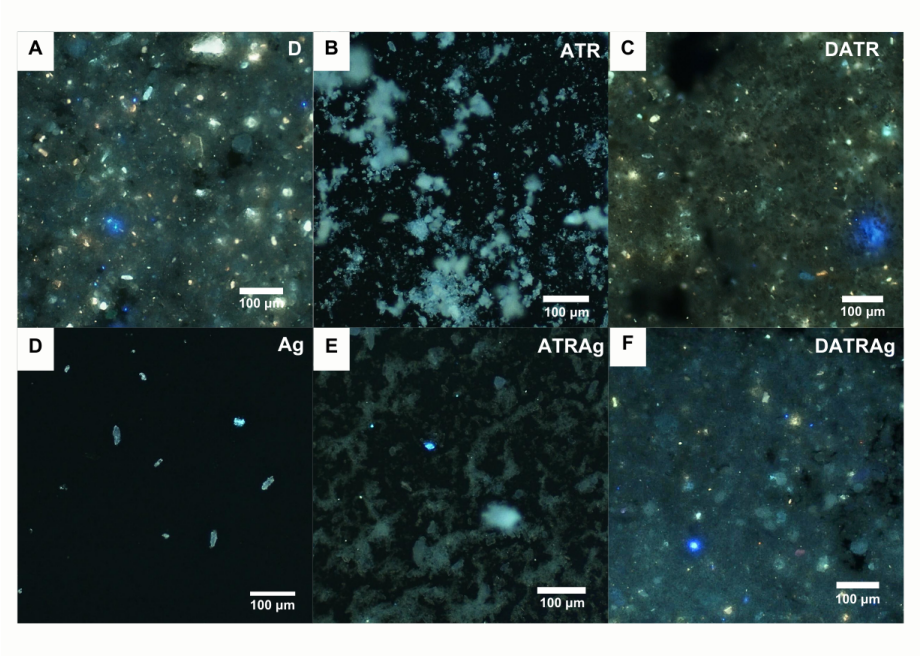

Figure 5.10: Fluorescence Micrographs of **(A)** diatoms, **(B)** atrazine, **(C)** diatoms + atrazine, **(D)** AgNPs, **(E)** AgNPs + atrazine, and **(F)** Diatoms doped with AgNPs + atrazine.

the atrazine (E) there are no significant changes from the one of atrazine alone (B). Finally, in comparison with the sample of diatoms with atrazine (C) and the diatoms doped with AgNPs + atrazine (F), it is observed a little enhancement in the fluorescence in comparison of diatoms (A) and atrazine (B) showing the enhancement of fluorescence due to the diatoms doped with AgNPs.

Figure 5.11 shows the fluorescence microscopy of AuNPs (D). Compared with the diatoms doped with AgNPs, this sample shows a strong fluorescence in contact with atrazine, in agreement with Raman's results. The fluoresce response of the diatoms decorated with gold nanoparticles is explained when the incident light leads to excitation of the surface plasmon coherent electronic motion as well as the d electrons which is in agreement with Briceno, et al analysis.[101] Then, the sample of AuNPs with atrazine (E) in comparison with atrazine (B) is observed, also an enhancement in the fluorescence of the sample in some localized areas. Finally, the sample of diatoms doped with gold nanoparticles in contact with atrazine (F) presented a higher fluorescence than all the other samples, even in comparison with the sample of diatoms doped with AgNPs in contact with atrazine.

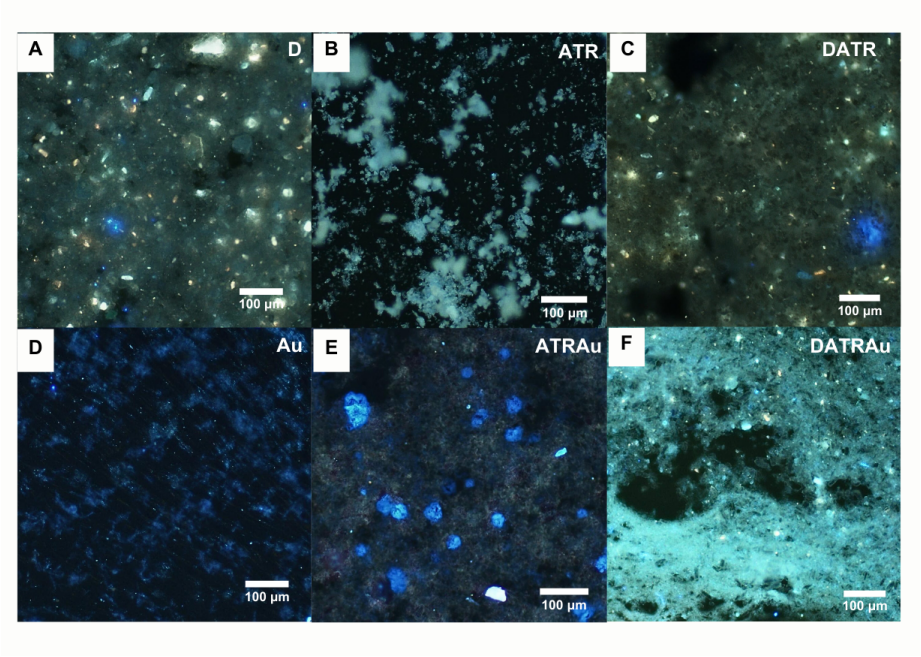

Figure 5.11: Fluorescence Micrographs of **(A)** diatoms, **(B)** atrazine, **(C)** diatoms + atrazine, **(D)** AuNPs, **(E)** AuNPs + atrazine, and **(F)** Diatoms doped with AuNPs + atrazine.

5.7 Atrazine adsorption

5.7.1 Calibration curves

The calibration curves that were mentioned in the methodology it represented in order to achieve and determine the best concentrations of atrazine and diatoms, as well as the pH of working in the process of adsorption of atrazine using diatoms doped with gold or silver nanoparticles. In Figure 5.12, the calibration curve of the diatoms concentration with atrazine before a saturation value for detection. The different concentrations were dispersed in 10 mL of distilled water; 0.01 g, 0.025 g, 0.05 g, 0.075 g, and 0.1 g of diatoms. As it is shown over the concentration of 0.1 g of diatoms, absorbance goes above 1, showing saturation of the solution. Figure 5.13 shows the calibration curve of atrazine concentration. The different concentrations were dissolved in 10 mL of distilled water; 0.01 g, 0.025 g, 0.05 g, 0.075 g, and 0.1 g of atrazine. As it is shown over the concentration of 0.05 g of atrazine, absorbance goes above 1, showing a saturation of the solution.

From these calibration experiments, the concentration of diatoms and atrazine used in the whole experimentation for the adsorption is determined in the following section. From Agdi, et al in which experiments use diatoms for the adsorption of atrazine, the concentration determined to use is 0.01 g of diatoms with 0.01 g of atrazine in an aqueous

solution of distilled water[120], in this case the volume of water is adjusted to 10 mL.

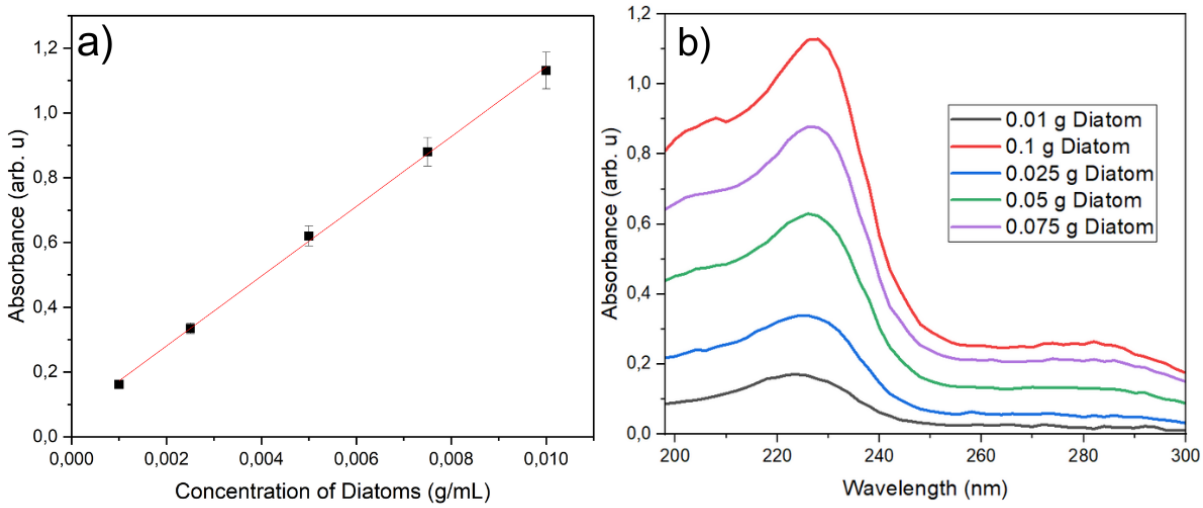

Figure 5.12: Calibration curve of diatoms with atrazine; **a)** Absorbance at a given wavelength vs. concentration of diatoms**b)** Absorption spectra of atrazine with diatoms at different concentrations of diatoms.

5.7.2 Effect of pH on adsorption

The pH of atrazine solutions was adjusted to 2, 4, 5, 8, and 11 with H_2SO_4 or NaOH, and the solutions were treated as it was described in the methodology section, in the subsection of the atrazine adsorption process.

In Figure 5.14, the results of the effect of pH are shown. In each of them, initial and final absorbance is observed in 4 hours of contact time between diatoms and atrazine. The sample in pH 5 (b) is the one from the solution without any adjusting performed with atrazine and distilled water. Agdi, et al. report since atrazine is a weak base, at acidic pH, it is in cationic form, indicating that ionic groups retain atrazine present in diatoms frustules[120]. That is why for the following experiments of adsorption, the natural pH of atrazine in water (5 pH) is used, due to the no significant changes from the other pH shown in Figure 5.14-f.

5.7.3 Adsorption process using diatoms

In Figure 5.15, the adsorption process of atrazine in water using diatoms was performed. The adsorption of the atrazine process for 4 days (4320 min) shows the standard solution of atrazine in distilled water in 5.15-a at 0 min,

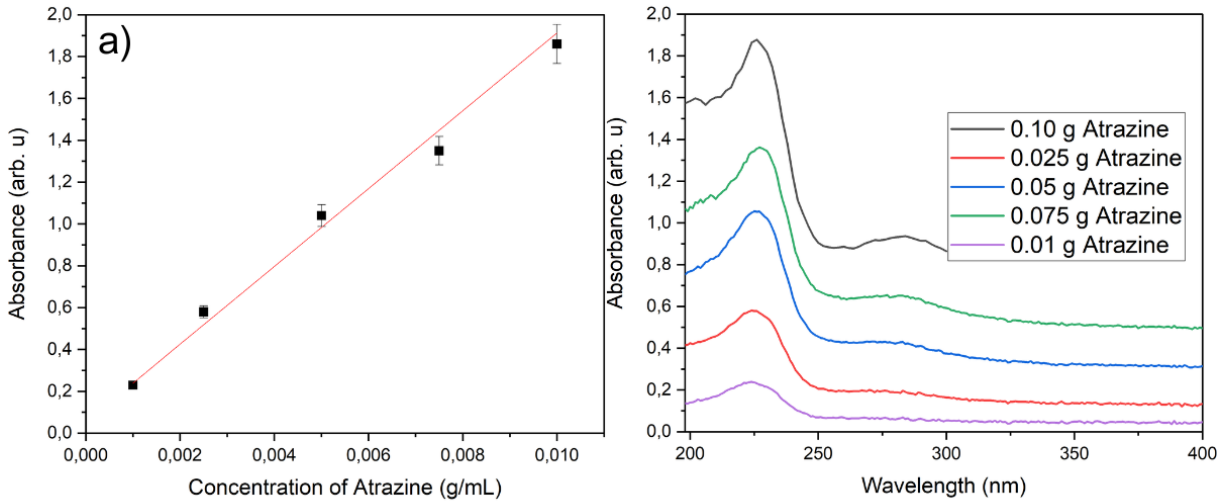

Figure 5.13: Calibration curve of concentration atrazine; **a)** Absorbance at a given wavelength vs. concentration of atrazine**b)** Absorption spectra of atrazine at different concentrations.

which is the baseline before the addition of 0.01 g of diatoms. It can be observed the decrease in the absorbance peak of atrazine at 226 nm with the exposition time, the stabilizing of the absorbance changes reaches after the first 2 days (1440-2880 min) shown in Figure 5.15-b and it finished at 4320 min. This behavior is explained by atrazine molecules binding to the diatom surface during the adsorption process. Furthermore, in Figure 5.15-c, it is observed the adsorption percentage reached at 4320 min of the contact time with diatoms in distilled water. This graph shows that at that time, it reached a maximum of 25.36% of adsorption. Then, in Figure 5.15-d, the amount of atrazine adsorbed was plotted, showing a mass of 25.36 mg of atrazine adsorbed by 0.01 g of diatoms.

5.7.4 Adsorption process using diatoms decorated with 0.01 mL of an AgNPs solution

In Figure 5.16, the adsorption process of atrazine in water using diatoms decorated with 0.01 mL of AgNPs was performed. The adsorption of the atrazine process for 4 days (4320 min) shows the standard solution of atrazine in distilled water in 5.16-a at 0 min, which is the initial before the addition of 0.01 g of AgNPs-diatoms. It can be observed the decrease in the absorbance peak of atrazine at 226 nm with the exposition time, the stabilizing of the absorbance changes reaches after the first 2 days (1440-2880 min) shown in Figure 5.16-b. This behavior can be explained by the fact that during the adsorption process, atrazine molecules are attaching at the surface of the diatoms

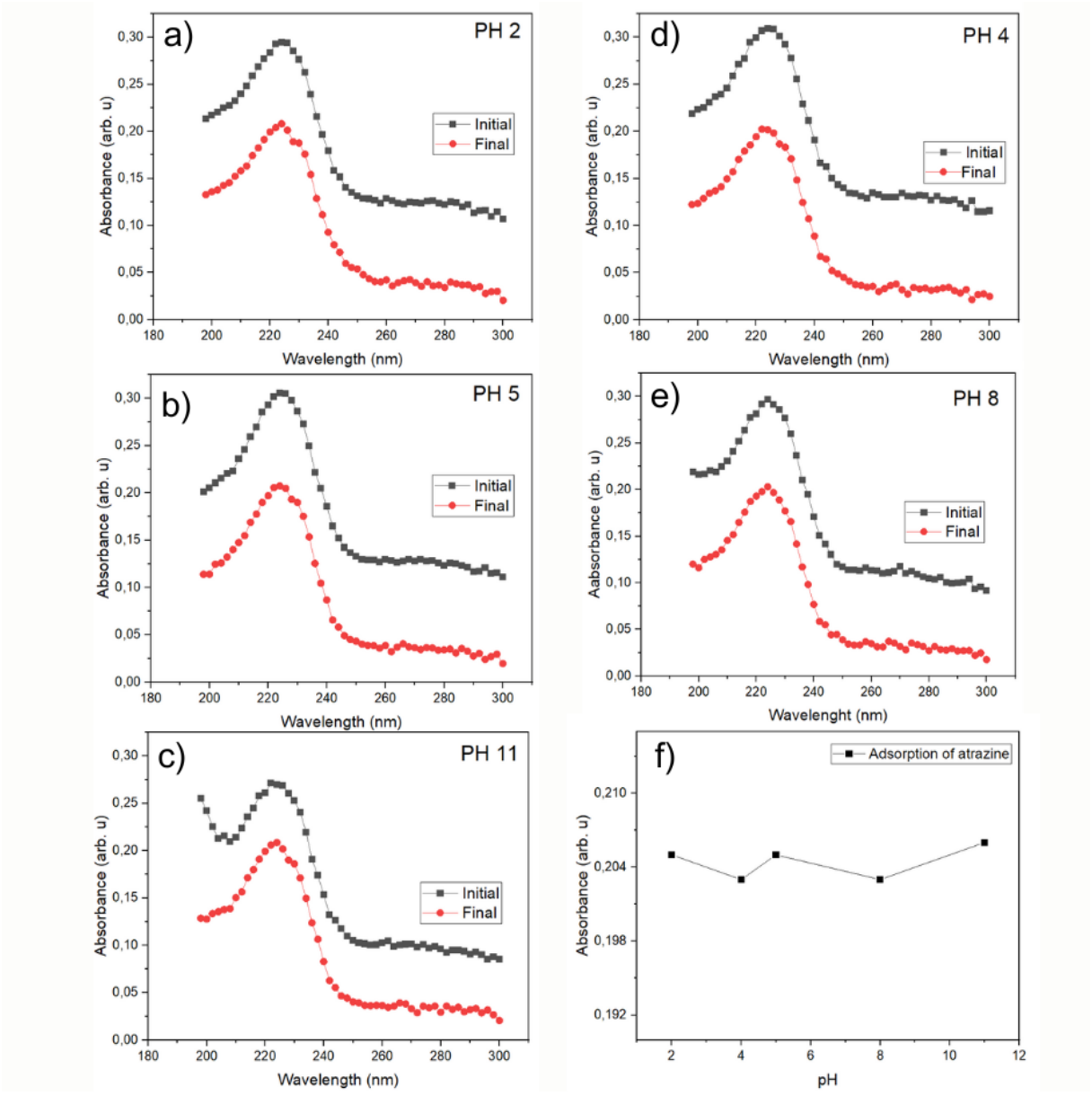

Figure 5.14: Calibration curve of atrazine adsorption using diatom in function pH; **a)** at pH 2, **b)** at pH 5, **c)** at pH 11, **d)** at pH 4, **e** at pH 8, **f)** Absorbance at a given wavelength vs. pH.

decorated with AgNPs. Furthermore, in Figure 5.16-c, it is observed the adsorption percentage reached during 4320 min of the contact time. This graph shows that at that time, it reaches a maximum of 22,18% of adsorption. Then,

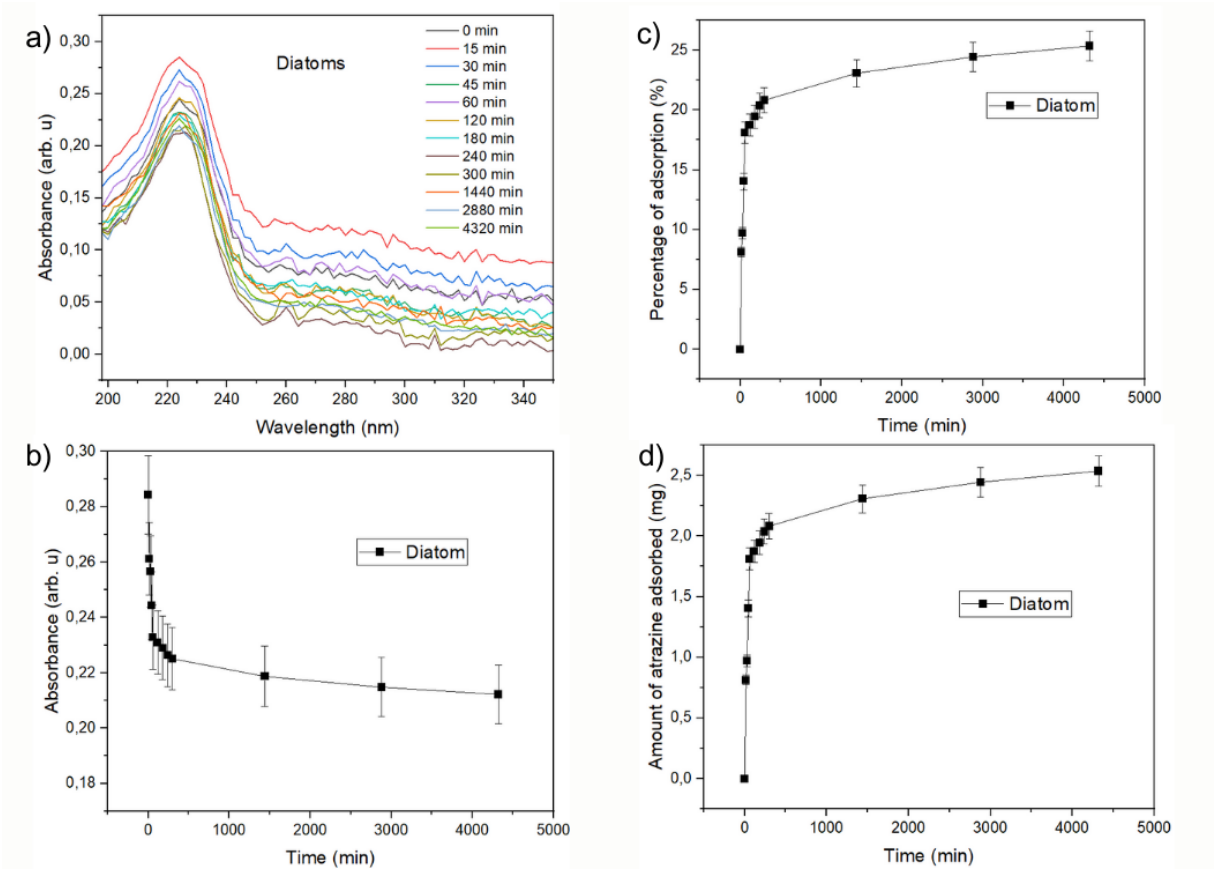

Figure 5.15: Atrazine adsorption using diatoms, a) Adsorption spectra of atrazine using diatoms in 4 days (4320 min), b) Absorbance at a given wavelength vs. time c) Percentage of adsorption vs. time, d) Amount of atrazine adsorbed vs. time

in Figure 5.16-d, the amount of atrazine adsorbed was plotted, showing a mass of 22.18 mg of atrazine adsorbed by 0.01 g of diatoms decorated with 0,01 mL of AgNPs.

5.7.5 Adsorption process using diatoms decorated with 0.05 mL of a AgNPs solution

The third sample using diatoms decorated with 0.05 mL of AgNPs behaves as previously described; using the absorbance peak of reference from atrazine at 226 nm, the adsorption efficiency was determined. In Figure 5.17-a and 5.17-b, it is observed that the process is stabilized between the first 3 days (2880 - 4320 min). Moreover, in Figure 5.17-c, it is observed the adsorption percentage reached after 4320 min of contact time with diatoms decorated with 0.05 mL of a solution of AgNPs in the solution of distilled water, reaching a maximum adsorption of 29.77%. Then, in Figure 5.17-d, the amount of atrazine adsorbed was plotted, showing a mass of 29.77 mg of atrazine adsorbed by

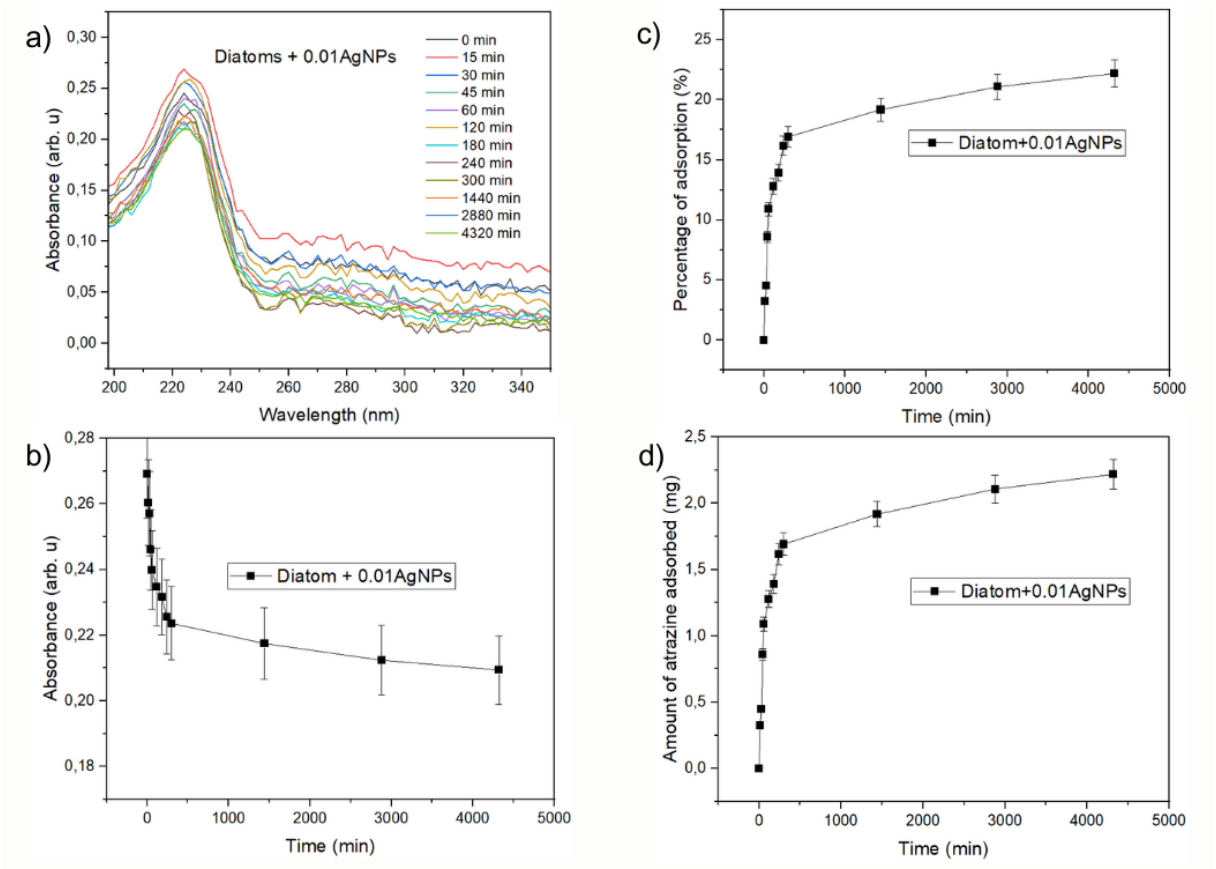

Figure 5.16: Atrazine adsorption using diatoms with 0,01 AgNPs, a) Adsorption spectra of atrazine using diatoms in 4 days (4320 min), b) Absorbance at a given wavelength vs. time c) Percentage of adsorption vs. time, d) Amount of atrazine adsorbed vs. time

0.01 g of diatoms decorated with 0,05 mL of AgNPs. From this, it was determined that with this sample, atrazine is adsorbed in a greater period of contact time, and in comparison with the sample of 0.01 mL AgNPs, the sample with 0,05 mL AgNPs, enhanced the adsorption of atrazine. This probably can be attributed to the fact that there are more AgNPs on the surface of diatoms, enhancing the interactions by the surface of diatoms decorated with atrazine molecules.

5.7.6 Adsorption process using diatoms decorated with 0.01 mL of AuNPs solution

For the usage of diatoms decorated with 0.01 mL of AuNPs, the results are similar to the ones previously described for diatoms decorated with 0.05 mL of AgNPs. In Figure 5.18-a and 5.18-b, it is observed that the adsorption process is stabilized in the first 3 days (2880 - 4320 min). Hence, here, using less solution of AuNPs in comparison

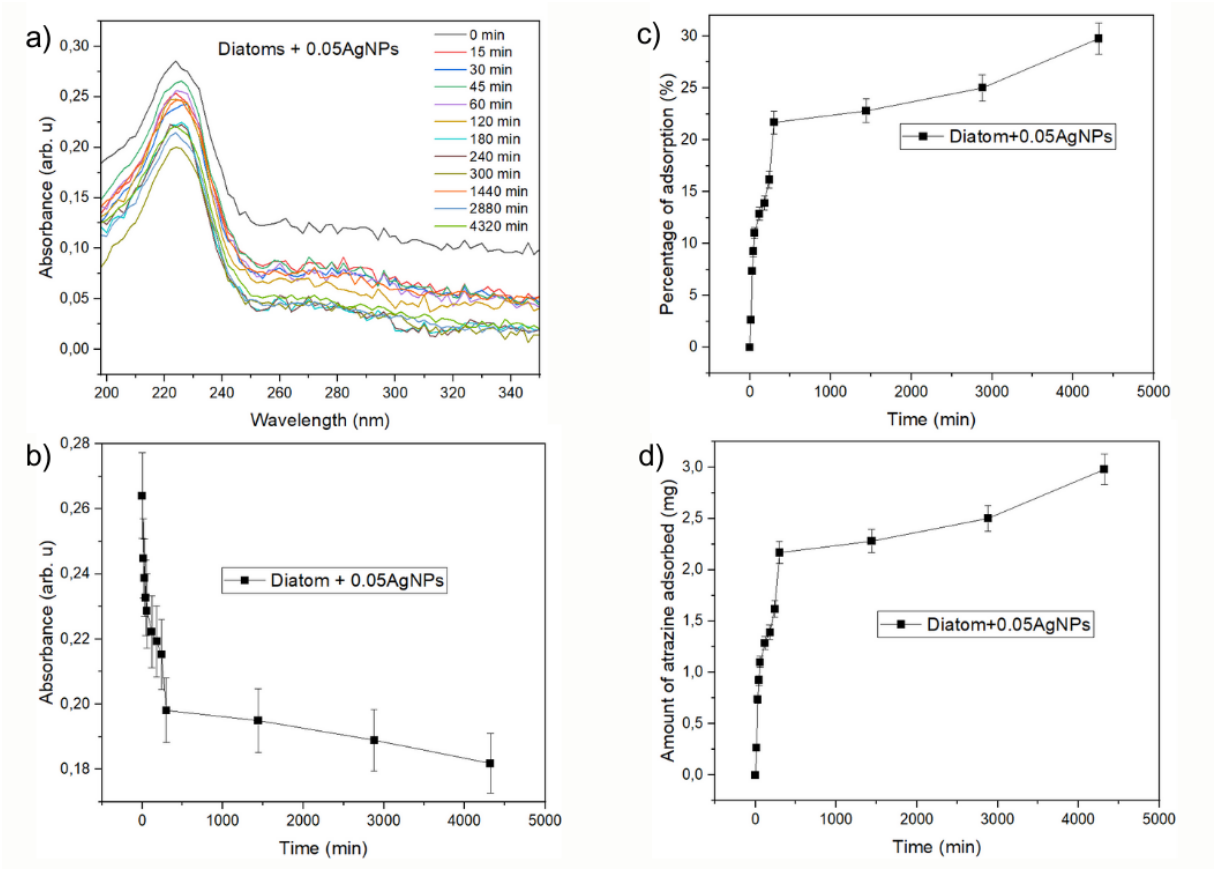

Figure 5.17: Atrazine adsorption using diatoms with 0.05 AgNPs, a) Adsorption spectra of atrazine using diatoms in 4 days (4320 min), b) Absorbance at a given wavelength vs. time c) Percentage of adsorption vs. time, d) Amount of atrazine adsorbed vs. time

with the sample described before in Figure 5.17, the adsorption is similar. In this case, the adsorption percentage reached after 4320 min of contact time with diatoms decorated with 0.01 mL of AuNPs in distilled water, reaching a maximum of 29.32% of adsorption. Then, in Figure 5.18-d, the amount of atrazine adsorbed was plotted, showing a mass of 29.32 mg of atrazine adsorbed by 0.01 g of diatoms decorated with 0.01 mL of AuNPs.

5.7.7 Adsorption process using diatoms decorated with 0.05 mL of AuNPs solution

For the sample of diatoms decorated with 0.05 mL of AuNPs, the adsorption process was enhanced than the previous sample. In Figure 5.19-a and Figure 5.19-b, the adsorption behavior and how it is stabilized after 3 days as well as with the 2 previous samples (2880 - 4320 min). The adsorbed percentage and mass adsorbed of atrazine with these decorated diatoms is observed in Figure 5.19-c and Figure 5.19-d. The adsorption percentage after 4320 min

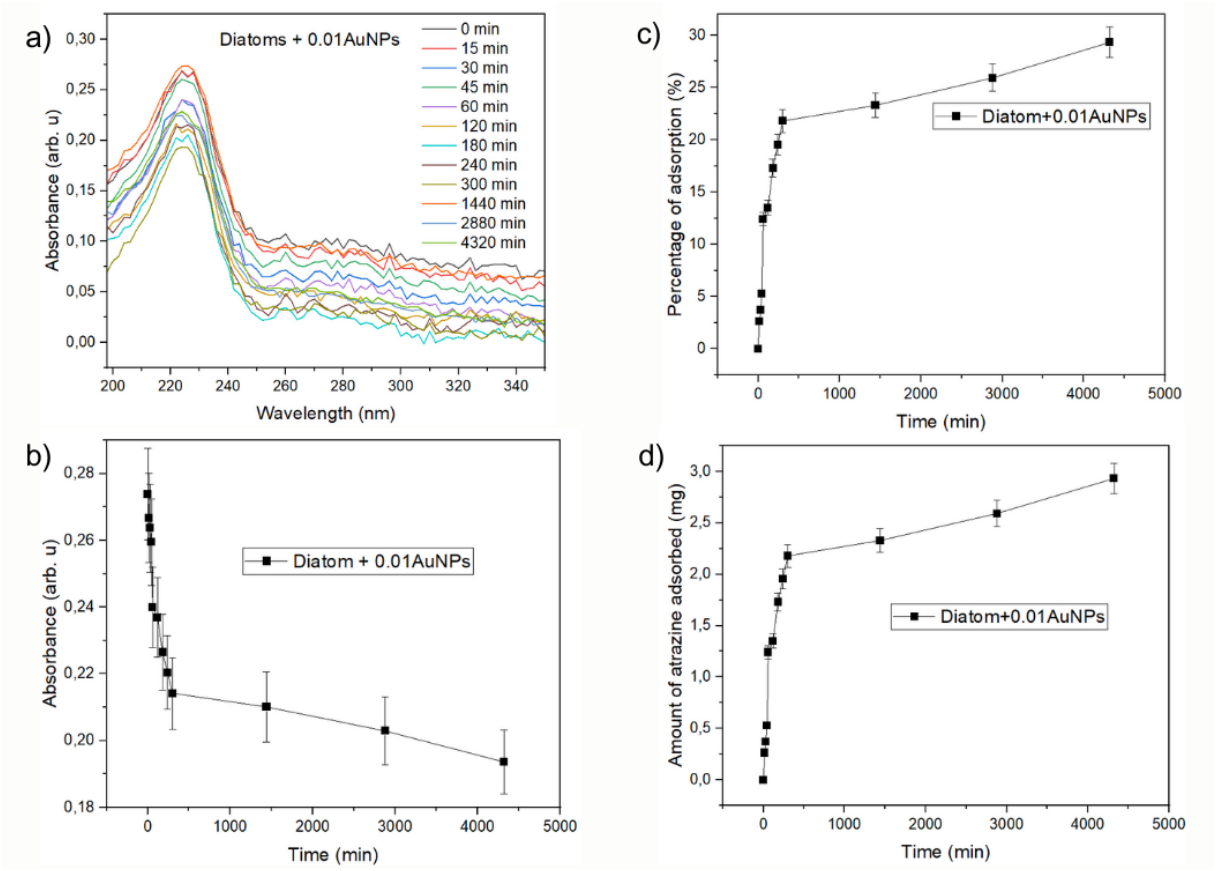

Figure 5.18: Atrazine adsorption using diatoms, a) Adsorption spectra of atrazine using diatoms with 0.01 AuNPs in 4 days (4320 min), b) Absorbance at a given wavelength vs. time c) Percentage of adsorption vs. time, d) Amount of atrazine adsorbed vs. time

of the contact time with diatoms decorated with 0.05 mL of AuNPs in the distilled water reaches a maximum of 31.12% of adsorption. Then, in Figure 5.19-d, the amount of atrazine adsorbed was plotted, showing a mass of 31.12 mg of atrazine adsorbed by 0.01 g of diatoms decorated with 0.05 mL of AuNPs. From this, the enhancement of atrazine adsorption performed by this sample can be attributed to an enhancement of the interactions between gold nanoparticles surface and atrazine molecules with diatoms that were previously described in the FTIR and Raman sections.

5.7.8 Adsorption Kinetics

Since all samples comes from diatoms with a decorated surface with a small concentration of nanoparticles on it, the adsorption kinetics are compared between them if the behaviour fits with each of them and to describe the adsorption

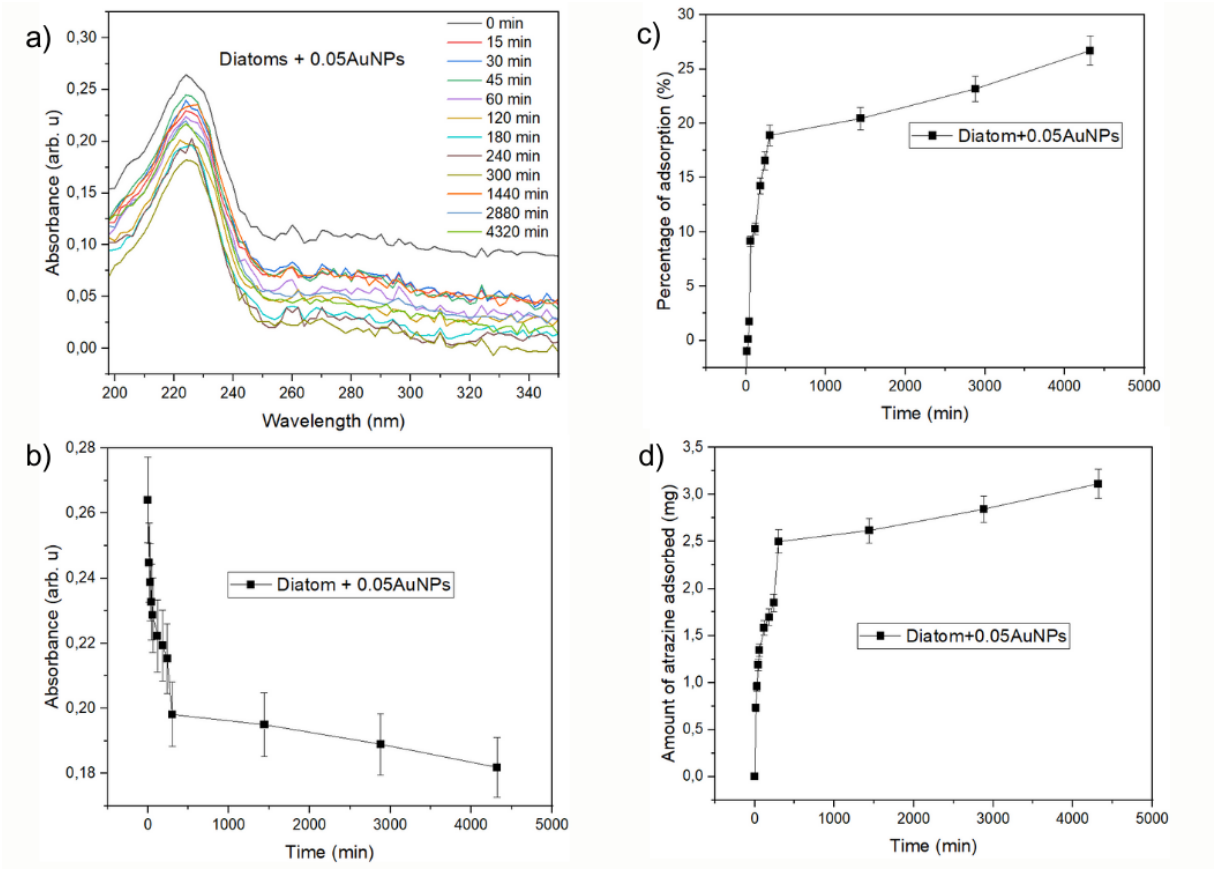

Figure 5.19: Atrazine adsorption using diatoms with 0.05 mL of AuNPs, a) Adsorption spectra of atrazine using diatoms after 4 days (4320 min), b) Absorbance at a given wavelength vs. time c) Percentage of adsorption vs. time, d) Amount of atrazine adsorbed vs. time

process occurs with atrazine on decorated diatoms. In Figure 5.20 a) it is plotted the linear regression of pseudo first order kinetic model from which adjustments fits well with all the samples. Then, in Figure 5.20 b) it is plotted the linear regression of the pseudo second order kinetic model fitting better than the pseudo first order with all the samples used (diatoms and decorated diatoms at different concentration of diatoms).

In Table 5.4 it is tabulated the adsorption rate constant of each model (PFO and PSO) at the same time it is tabulated the values of the correlation fitting values R^2 from which it is determined the best fitting model for the experimental data provided. In all case of samples including diatoms and diatoms decorated with different concentration of silver and gold nanoparticles the pseudo-second order model is obeyed. From this analysis it indicates that chemisorption is the rate controlling step for these adsorption.[76]. This provides a stronger bond as

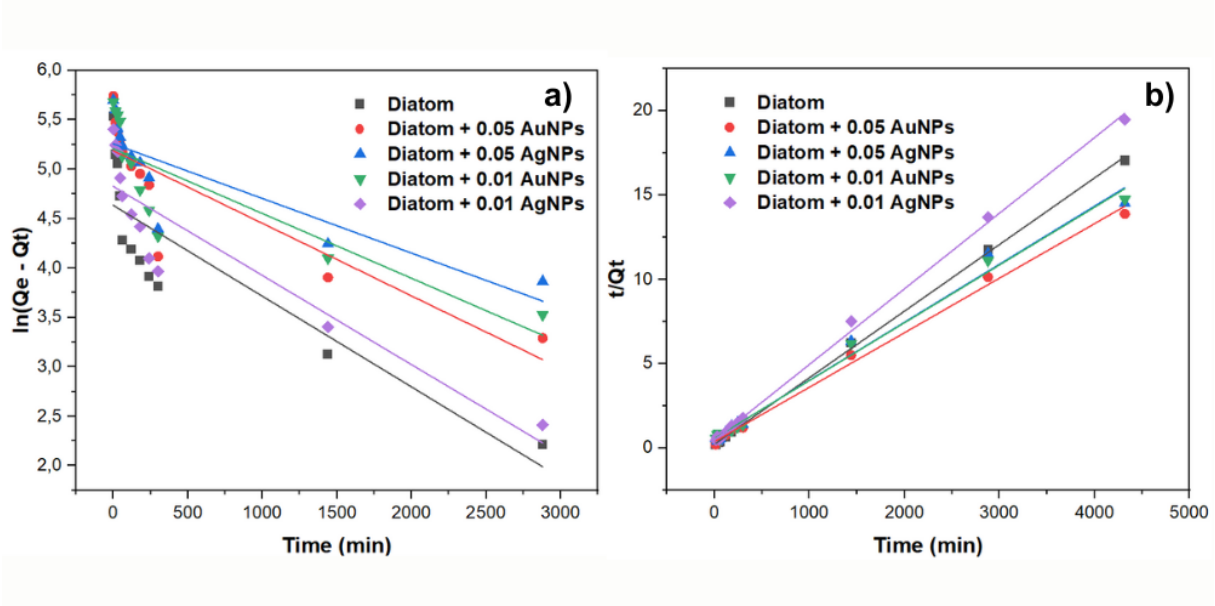

Figure 5.20: **a)** Pseudo First Order and **b)** pseudo second order kinetics plots for atrazine adsorption process.

it involves the transfer or sharing of electrons between the commercial diatoms and diatoms nanocomposites. It is important to mention that for all samples the values of k1 and k2 (Table 5.4) constants are in accordance with the ones reported by Tan k. et al.,[74] which affirm that the rate constant k1 is a function of the process conditions due to decrease with increasing initial bulk concentration.[73,74]

Table 5.4: Adsorption Kinetics Model Parameters for each sample.

Sample	**Q_t (mg/g)**	**R (%)**	**Pseudo First Order Kinetics (PSO)**		**Pseudo Second Order Kinetics (PSO)**	
			k_1 (min^{-1})	**R^2**	**k_2 (g/mg.min)**	**R^2**
Diatom	253.6	25.36	$-9.18x10^{-4}$	0.74	$3.95x10^{-3}$	0.99
DAG01	221.85	22.18	$-9.01x10^{-4}$	0.82	$4.48x10^{-3}$	0.99
DAU01	293.17	29.31	$-6.55x10^{-4}$	0.70	$3.43x10^{-3}$	0.99
DAG05	297.79	29.77	$-5.52x10^{-4}$	0.71	$3.44x10^{-3}$	0.99
DAU05	311.24	31.12	$-7.34x10^{-4}$	0.76	$3.23x10^{-3}$	0.99

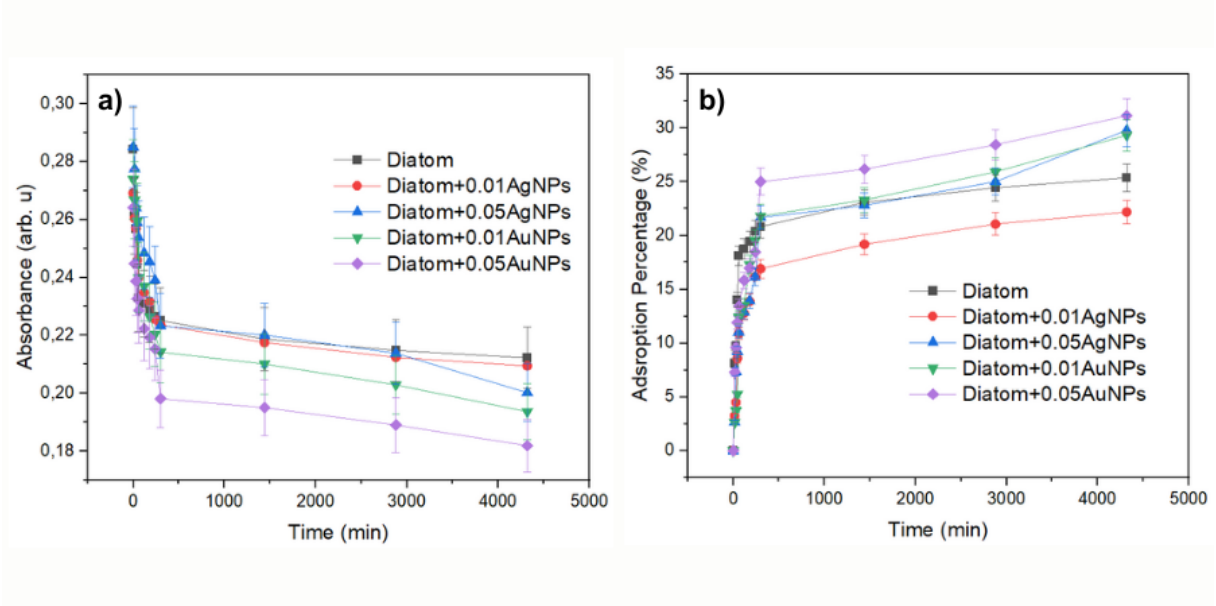

Figure 5.21: Atrazine adsorption using diatoms with AgNPs or AuNPs, a) Absorbance at a given wavelength vs. time b) Percentage of adsorption vs. time.

5.7.9 Adsorption process comparison within the samples

Finally, this section shows the comparison between the samples. Figure 5.21-a shows the absorbance vs. time, and Figure 5.21-b presents the percentage of adsorption vs. time. For the analysis, it is important to focus that in the first 4 hours, the five samples behave similarly to each other, and the significant changes come from the first day (1440 min). Then, the contact time with samples is important to take into account for the adsorption process. Moreover, after the 4320 min has finished, the sample with the less absorbance is the sample of diatoms decorated with 0.05 mL of AuNPs, which has the higher adsorption percentage of atrazine. The values to be compared are shown in Table 5.5 as well as it comparison graphically in Figure 5.22.

Table 5.5: Results of adsorption efficiency after 4320 min of contact time with all the samples.

	Final Adsorption Percentage	Final mass of atrazine adsorbed
Sample	(%)	(mg)
D	25.36	25.36
DAG01	22.18	22.18
DAG05	29.77	29.77
DAU01	29.32	29.32
DAU05	31.12	31.12

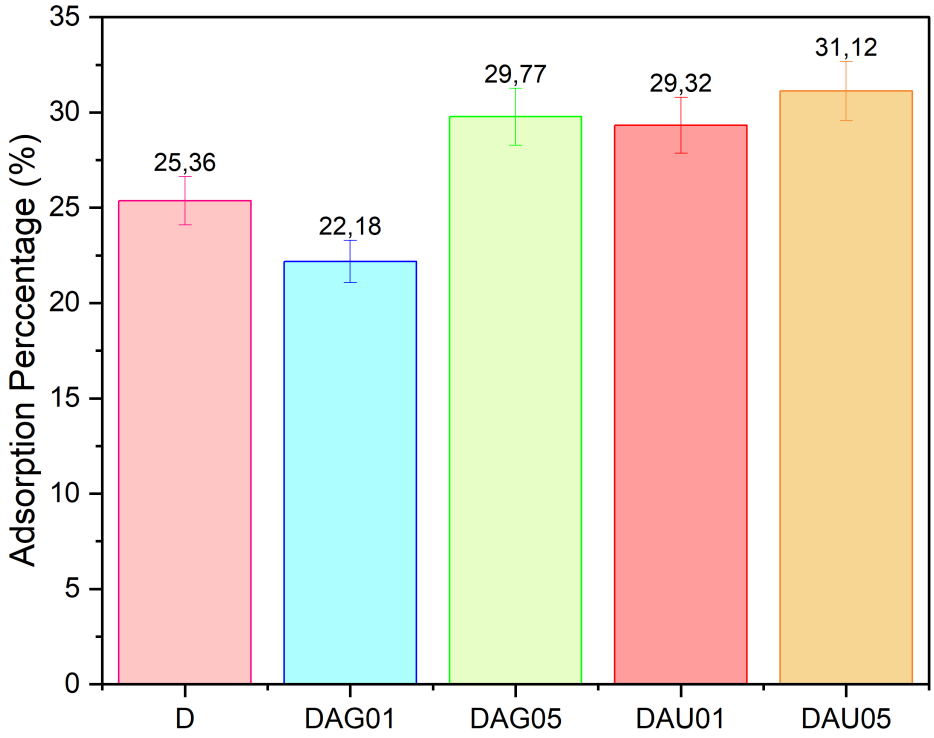

Figure 5.22: Results of atrazine adsorption efficiency after 4320 min of contact time with all the samples

Chapter 6

Conclusions & Outlook

This work studied the adsorption process of diatoms doped with gold or silver nanoparticles, respectively. For the usage of diatoms, specifically, *Aulacoseira* diatoms collected from the valley of Guallyabamba. The diatoms frustules obtained from this location show a tubular form with an ordered pore arrangement characterized using SEM in which the tubular shape of an average size of 26.76 μm and an average pore size of 500 nm. EDX results indicate the main composition of these diatom frustules: of SiO_2 and aluminum. UV-Vis spectroscopy confirmed the formation of the nanoparticles with an absorbance band of 404 nm for silver nanoparticles and 525 nm for gold nanoparticles. The analysis of SEM and EDX confirmed the distribution of the nanoparticles on the diatom frustules.

The analysis done by FTIR characterization showed the interactions between diatoms deocrated with nanoparticles as well as the interaction in the process of adsorption with these samples that due to nitrogen functional groups with the surface of diatoms and CTAB capped surface of AuNPs as well as the citrate capped surface of AgNPs enhance the interaction of diatoms in the adsorption of atrazine. Moreover, this interaction was also confirmed by Raman spectroscopy as well as the SERS effect obtained from them not only in the adsorption of atrazine but also for the enhancement of its Raman signal attributed to the surface plasmon resonance of the metallic nanoparticles used. Additionally, the optical properties of diatoms decorated with nanoparticles, in particular fluorescence, were also confirmed by Raman and fluorescence microscopy due to this interaction of gold and silver nanoparticles with atrazine molecules.

The adsorption process of atrazine using different samples with two different concentrations of gold and silver nanoparticles and its comparison with non-doped diatoms was performed and analyzed using UV-Vis spectroscopy in the analysis of its absorbance during a period of time of 4 days. The atrazine kientics adsorption results of the samples, correspond to a pseudo-second-order kinetic model, being controlled by the chemisorption process. In this analysis, it was demonstrated the efficient adsorption of atrazine using diatoms decorated with nanoparticles. The DAU05 sample is the one that shows the highest percentage of adsorption between the other ones of an efficiency percentage of 31.12 in 4 days, demonstrating that AuNPs enhances the adsorption of atrazine.

This work contributes to the use of natural biomaterials from Ecuador for water remediation applications and its understanding of its optical properties that can help in the detection of pesticides in water and other biosensor applications. For further research, it is recommended to improve the contact time in order to make the adsorption efficiency in less time than it was performed in this work. Additionally, the temperature could be an important factor that should be taken into account in future works. Moreover, a deeper characterization of molecule interaction is recommended to determine which specific functional groups interact with the doped-diatom surfaces.

Bibliography

[1] Smol, J. P.; Stoermer, E. F. *The diatoms: applications for the environmental and earth sciences*; Cambridge University Press, 2010.

[2] Guzmán, M. G.; Dille, J.; Godet, S. Synthesis of silver nanoparticles by chemical reduction method and their antibacterial activity. *Int J Chem Biomol Eng* **2009**, *2*, 104–111.

[3] Smith, D. K.; Korgel, B. A. The importance of the CTAB surfactant on the colloidal seed-mediated synthesis of gold nanorods. *Langmuir* **2008**, *24*, 644–649.

[4] Netto, M. S.; Georgin, J.; Franco, D. S.; Mallmann, E. S.; Foletto, E. L.; Godinho, M.; Pinto, D.; Dotto, G. L. Effective adsorptive removal of atrazine herbicide in river waters by a novel hydrochar derived from Prunus serrulata bark. *Environmental Science and Pollution Research* **2022**, *29*, 3672–3685.

[5] Pannico, M.; Rea, I.; Chandrasekaran, S.; Musto, P.; Voelcker, N. H.; De Stefano, L. Electroless gold-modified diatoms as surface-enhanced Raman scattering supports. *Nanoscale research letters* **2016**, *11*, 1–6.

[6] Gutu, T.; Gale, D. K.; Jeffryes, C.; Wang, W.; Chang, C.-h.; Rorrer, G. L.; Jiao, J. Electron microscopy and optical characterization of cadmium sulphide nanocrystals deposited on the patterned surface of diatom biosilica. *Journal of Nanomaterials* **2009**, *2009*, 1–7.

[7] León-Valencia, A.; Briceño, S.; Reinoso, C.; Vizuete, K.; Debut, A.; Caetano, M.; González, G. Photochemical Reduction of Silver Nanoparticles on Diatoms. *Marine Drugs* **2023**, *21*, 185.

[8] Viji, S.; Anbazhagi, M.; Ponpandian, N.; Mangalaraj, D.; Jeyanthi, S.; Santhanam, P.; Devi, A. S.; Viswanathan, C. Diatom-based label-free optical biosensor for biomolecules. *Applied biochemistry and biotechnology* **2014**, *174*, 1166–1173.

[9] Lebeau, T.; Robert, S.; Laroche, C. Applications of diatoms in biotechnology. *Journal of Applied Phycology* **2008**, *20*, 577–590.

[10] Chen, X.; Shen, P. K.; Xia, X.; Wang, X.; Cui, Z.; Chen, X.; Chen, L.; Zhang, W.; Li, G. Diatom silica immobilized TiO2 for efficient removal of Cd (II) ions from wastewater. *Journal of Hazardous Materials* **2013**, *263*, 352–359.

[11] Wu, Y.; Wu, D.; Wu, P.; Liu, X.; Zhang, D.; Zhao, Y.; Chen, J.; Lin, J. Biosorption of heavy metals by diatomite and its potential application in water treatment: a review. *Water science and technology* **2016**, *74*, 1133–1147.

[12] Jiao, J.; Zhang, J.; Huang, G. Assessment of atrazine removal by algae-based systems: Performance, mechanisms, and environmental impacts. *Journal of Cleaner Production* **2021**, *309*, 1682–1697.

[13] Qu, X.; Liu, X.; Li, D.; Zhang, K.; Zeng, G. Simultaneous adsorption and degradation of atrazine in wastewater by granulated diatomite-supported TiO2 photocatalyst. *Journal of Hazardous Materials* **2020**, *384*, 121405.

[14] Daughton, C. G.; Ternes, T. A. Atrazine: environmental characteristics and ecological effects. *Reviews of environmental contamination and toxicology* **2003**, *179*, 1–154.

[15] Gevao, B.; Semple, K. T.; Jones, K. C.; Burauel, P. Atrazine transport in soil and its dependence on solution chemistry. *Environmental science technology* **2003**, *37*, 1752–1758.

[16] Mokhtar, M. M.; Abdalla, A. M. Atrazine in water resources and its removal methods: A review. *Journal of Water Process Engineering* **2021**, *39*, 101893.

[17] Liu, D.; Liu, F.; Yao, J.; Hu, J.; Huang, G. Efficient removal of Pb(II) from aqueous solution by diatomite supported on modified hydroxyapatite: Adsorption behavior and mechanism. *Chemosphere* **2020**, *250*, 126278.

[18] Zhang, Y.; Liu, J.; Li, Y.; Guo, J.; Li, Z. Review on adsorption of herbicides from water by different adsorbents. *Chemical Engineering Journal* **2021**, *414*, 128902.

[19] Armbrust, E. V. The life of diatoms in the world's oceans. *Nature* **2009**, *459*, 185–192.

[20] Falkowski, P. G.; Barber, R. T.; Smetacek, V. Biogeochemical controls and feedbacks on ocean primary production. *Science* **2004**, *281*, 200–206.

[21] Round, F.; Crawford, R.; Mann, D. The Diatom Book. **1990**,

[22] Kelly, M. G. Short term dynamics of diatoms in an upland stream and implications for monitoring eutrophication. *Environmental Pollution* **2003**, *125*, 117–122.

[23] Mehmood, A.; Song, Y.; Hao, X.; Zhang, X.; Wang, C.; Wang, P.; Gao, B.; Li, Y.; Wang, D. Adsorption of atrazine onto FeCl3-modified diatomite. *Environmental Science and Pollution Research* **2018**, *25*, 3702–3712.

[24] others,, *et al.* Evolution and metabolic significance of the urea cycle in photosynthetic diatoms. *Nature* **2008**, *473*, 203–207.

[25] Kr"oger, N. Diatoms, silica deposition and biomineralization. *New Phytologist* **2012**, *194*, 939–941.

[26] Kr"oger, N.; Poulsen, N.; Iversen, J. J. Silica morphogenesis by diatoms: new insights from the model organism Thalassiosira pseudonana. *Journal of Biological Chemistry* **2016**, *291*, 23539–23545.

[27] Sambrook, J.; Russell, D. W. Molecular cloning: a laboratory manual. **2001**,

[28] Brzezinski, M. A. The Si:C:N ratio of marine diatoms: interspecific variability and the effect of some environmental variables. *Journal of Phycology* **1985**, *21*, 347–357.

[29] Smetacek, V. Diatoms and the ocean carbon cycle. *Protist* **1999**, *150*, 25–32.

[30] Crawford, R. M. The diatoms: biology and morphology of the genera. *Cambridge University Press* **1991**,

[31] others,, *et al.* Ecology and distribution of Aulacoseira species (Bacillariophyta) in tropical reservoirs from Brazil. *Diatom Research* **2016**, *31*, 199–215.

[32] Chico, C.; Anai, E. Use of Natural Diatoms doped with gold nanoparticles for Gentamicin Drug Delivery. B.S. thesis, Universidad de Investigación de Tecnología Experimental Yachay, 2020.

[33] Maldonado Pinos, P. N. Natural and doped diatoms for photodegradation under visible light. B.S. thesis, Universidad de Investigación de Tecnología Experimetal Yachay, 2020.

[34] Agency, U. S. E. P. Atrazine. `https://www.epa.gov/ingredients-used-pesticide-products/atrazine`, 2020.

[35] Solomon, K. R.; Carr, J. A.; Du Preez, L. H.; Giesy, J. P.; Kendall, R. J.; Smith, E. E.; et al., Effects of atrazine on fish, amphibians, and aquatic reptiles: a critical review. *Critical reviews in toxicology* **2008**, *38*, 721–772.

[36] Aryal, N.; Reinhard, M. Atrazine degradation in aquatic systems: a review. *Journal of environmental science and health. Part. B, Pesticides, food contaminants, and agricultural wastes* **2010**, *45*, 1–29.

[37] Scribner, E. A.; Battaglin, W. A.; Goolsby, D. A.; Thurman, E. M. Atrazine in surface water and groundwater: a review of current research. *Journal of environmental quality* **2020**, *49*, 825–835.

[38] for Research on Cancer, I. A. *IARC Monographs Volume 112: evaluation of five organophosphate insecticides and herbicides*; International Agency for Research on Cancer: Lyon, France, 2015.

[39] Hayes, T. B.; Anderson, L. L.; Beasley, V. R.; de Solla, S. R.; Iguchi, T.; Ingraham, H.; et al., Demasculinization and feminization of male gonads by atrazine: consistent effects across vertebrate classes. *The Journal of steroid biochemistry and molecular biology* **2010**, *121*, 74–9.

[40] Bakshi, S.; Singh, R.; Kumar, R.; Bajpai, V. K.; Sastry, T. P.; Singh, R. P.; Tripathi, A. Gold nanoparticles: a paradigm shift in biomedical applications. *Advanced Materials Letters* **2014**, *5*, 97–108.

[41] Sastry, M. Biological Synthesis of Nanoparticles from Microorganisms and Plants. *Trends in Biotechnology* **2003**, *21*, 242–246.

[42] Khan, Z.; Singh, R.; Hussain, I.; Tanveer, M.; Tariq, M. Synthesis and characterization of silver nanoparticles for plant disease management: a comprehensive review. *Environmental Science and Pollution Research* **2019**, *26*, 17052–17065.

[43] Ahmed, S.; Annu,; Ikram, S.; Yudha S, S.; Ahmad, A.; Umar, S.; Wahab, R. Silver Nanoparticles: Synthesis, Characterization, Properties, Applications, and Therapeutic Approaches. *International Journal of Nanomedicine* **2016**, *11*, 1–19.

[44] Ghorbanzadeh, M.; Hadipour, N. L.; Rastegar, F.; Shokouhimehr, M.; Jafarian, M. Highly efficient removal of atrazine from water by metal-organic framework-coated diatomite. *Journal of Environmental Chemical Engineering* **2019**, *7*, 103278.

[45] Parnian, H.; Yaghmaeian, K.; Ahmadpour, A. Adsorption of atrazine by diatomite-modified natural zeolite: Kinetic, isotherm, and thermodynamic studies. *Environmental Research* **2020**, *185*, 109467.

[46] Shankar, S. S.; Rai, A.; Ankamwar, B.; Singh, A.; Ahmad, A.; Sastry, M. Biological synthesis of triangular gold nanoprisms. *Nature Materials* **2004**, *3*, 482–488.

[47] Li, N.; Sun, Y.; Zeng, Q.; Wang, J.; Li, M.; Zhang, Q.; Zhao, Y.; Li, J. Adsorption of atrazine from aqueous solution using chitosan-modified diatomite. *Journal of Environmental Sciences* **2018**, *63*, 86–95.

[48] Huang, Y.; Li, B.; Li, S.; Fang, Q.; Li, C.; Li, G. Recent advances in diatomite-based adsorbents for the removal of heavy metals and organic pollutants: A review. *Chemical Engineering Journal* **2021**, *416*, 129045.

[49] Chatterjee, D.; Dasgupta, S.; Nath, S.; Das, S.; Dey, S. K. A review on the advances of Gold nanoparticle in biomedical applications. *Chemical Biology and Drug Design* **2015**, *85*, 7–22.

[50] D'ıez-Pascual, A. M.; D'ıez-Vicente, A. L. Polypropylene/montmorillonite nanocomposites: a review of fabrication, characterization and applications. *Materials Science and Engineering: R: Reports* **2015**, *91*, 1–28.

[51] Akbarzadeh, O.; Yousefi, A. A. A review on the application of nanocomposites in food packaging. *Journal of Food Processing and Preservation* **2017**, *41*, e13291.

[52] Ghasemi, I.; Azizi, H.; Mohajeri, S. A review on the mechanical properties of polymer/clay and polymer/graphene nanocomposites. *Polymer Composites* **2016**, *37*, 2271–2285.

[53] Kausar, A.; Hussain, M. A.; Imran, M.; Siddiqi, H. M. Recent progress in synthesis and characterization of poly (vinyl alcohol)/clay nanocomposites. *Polymer Reviews* **2017**, *57*, 630–671.

[54] Rana, S.; Cho, J.-W.; Matsuura, T. A review of recent developments in the synthesis procedures and properties of graphene/polymer nanocomposites. *Composites Part A: Applied Science and Manufacturing* **2019**, *116*, 79–93.

[55] Joshi, M.; Dodiya, D. Nanocomposites for biomedical applications: a review. *Materials Science for Energy Technologies* **2019**, *2*, 100–108.

[56] Khoiruddin, S.; Purnawan, C. Preparation and characterization of polystyrene/nanosilica nanocomposites: a review. *Journal of Materials Research and Technology* **2019**, *8*, 1054–1064.

[57] Sing, K. S. W.; Everett, D. H.; Haul, R. A. W.; Moscou, L.; Pierotti, R. A.; Rouquerol, J.; Siemieniewska, T. Reporting physisorption data for gas/solid systems with special reference to the determination of surface area and porosity (Recommendations 1984). *Pure and Applied Chemistry* **1985**, *57*, 603–619.

[58] Nakamoto, K. *Infrared and Raman Spectra of Inorganic and Coordination Compounds*, 6th ed.; Wiley, 2009.

[59] Ruiz-Salvador, A. R.; Wiewiora, M. H.; Ramos-Fernandez, E. V. Porous materials in catalysis: challenges for mesoporous materials. *Chemical Society Reviews* **2016**, *45*, 4978–4999.

[60] Hapke, B. *Theory of reflectance and emittance spectroscopy*, 2nd ed.; Cambridge University Press, 1993.

[61] Cullity, B. D.; Stock, S. R. *Elements of X-ray Diffraction*, 3rd ed.; Prentice-Hall, 2001.

[62] Gregg, S. J.; Sing, K. S. W. *Adsorption, Surface Area, and Porosity*, 2nd ed.; Academic Press, 1982.

[63] Langmuir, I. The adsorption of gases on plane surfaces of glass, mica and platinum. *Journal of the American Chemical Society* **1918**, *40*, 1361–1403.

[64] Low, J. J.; Benin, A. I.; Jakubczak, P.; Abrahamian, J. F.; Willis, R. R. Large-scale synthesis of the metal-organic framework UiO-66. *Journal of Materials Chemistry* **2008**, *18*, 4387–4393.

[65] Trenor, S. R.; Wang, T. C.; Pinnau, I.; Long, J. R. Metal-organic framework materials for catalysis: advances and challenges. *Chemical Society Reviews* **2016**, *45*, 764–781.

[66] Wong, C.-H. Adsorption. *Encyclopedia of Life Sciences* **2001**, 1–6.

[67] Hildebrand, M. Biomineralization in diatoms: characterizing the intrinsic properties of silica nanostructures. *Proceedings of the National Academy of Sciences* **2008**, *105*, 839–840.

[68] Mann, D.; Droop, S. Chemical composition of diatom frustules. *Journal of Phycology* **2001**, *37*, 723–737.

[69] Hildebrand, M. Nanoporous silica from diatom biosilica. *Chemical Society Reviews* **2006**, *35*, 761–771.

[70] Miao, A.; Wang, W. Diatom-based biosorbents for the removal of heavy metals from water: A review. *Bioresource Technology* **2017**, *244*, 1407–1414.

[71] Patil, S.; Mone, M.; Kamat, V. Diatom biosilica-based drug delivery systems. *Expert Opinion on Drug Delivery* **2016**, *13*, 1121–1132.

[72] Natrajan, A.; Niederberger, M. Diatom silica: a smart material for drug delivery. *Advanced Healthcare Materials* **2017**, *6*, 1601300.

[73] Ho, Y.-S.; McKay, G. Pseudo-second order model for sorption processes. *Process biochemistry* **1999**, *34*, 451–465.

[74] Tan, K.; Hameed, B. Insight into the adsorption kinetics models for the removal of contaminants from aqueous solutions. *Journal of the Taiwan Institute of Chemical Engineers* **2017**, *74*, 25–48.

[75] Simonin, J.-P. On the comparison of pseudo-first order and pseudo-second order rate laws in the modeling of adsorption kinetics. *Chemical Engineering Journal* **2016**, *300*, 254–263.

[76] Mohammadi, A.; Aliakbarzadeh Karimi, A. Methylene blue removal using surface-modified TiO2 nanoparticles: a comparative study on adsorption and photocatalytic degradation. *Journal of Water and Environmental nanotechnology* **2017**, *2*, 118–128.

[77] Aharoni, C.; Sparks, D. L. Kinetics of soil chemical reactions—a theoretical treatment. *Rates of soil chemical processes* **1991**, *27*, 1–18.

[78] Harris, D. C. *Quantitative Chemical Analysis*, 8th ed.; W. H. Freeman, 2010.

[79] Skoog, D. A.; Holler, F. J.; Crouch, S. R. *Principles of Instrumental Analysis*, 6th ed.; Cengage Learning, 2013.

[80] Silverstein, R. M.; Webster, F. X.; Kiemle, D. J. *Spectrometric Identification of Organic Compounds*, 7th ed.; Wiley, 2004.

[81] Willard, H. H.; Merritt, L. L., Jr.; Dean, J. A., Jr.; Settle Jr., F. A. *Instrumental Methods of Analysis*, 7th ed.; Cengage Learning, 2004.

[82] Goldstein, J. I.; Newbury, D. E.; Echlin, P.; Joy, D. C.; Romig Jr., A. D.; Lyman, C. E.; Fiori, C. *Scanning Electron Microscopy and X-Ray Microanalysis*; Springer, 2018.

[83] Reimer, L.; Kohl, H. *Transmission Electron Microscopy: Physics of Image Formation and Microanalysis*; Springer Science Business Media, 2008.

[84] Mann, S., Ed. *Biomineralization: Principles and Concepts in Bioinorganic Materials Chemistry*; Oxford University Press, 2001.

[85] Losic, D.; Mitchell, J. G. *Nanotechnology: Science and Computation*; Springer, 2006; pp 59–77.

[86] Goldfarb, I.; Perez, R. *Scanning Electron Microscopy and X-Ray Microanalysis: A Text for Biologists, Materials Scientists, and Geologists*; Springer Science Business Media, 2006.

[87] Williams, D. B.; Carter, C. B. *Transmission Electron Microscopy: A Textbook for Materials Science*; Springer Science Business Media, 2009.

[88] Heinrich, K. F. *Handbook of X-ray Spectrometry: Methods and Techniques*; CRC Press, 2017.

[89] Smith, E.; Dent, G. *Modern Raman Spectroscopy: A Practical Approach*; John Wiley Sons, 2005.

[90] Kneipp, K.; Kneipp, H.; Itzkan, I.; Dasari, R. R.; Feld, M. S. Ultrasensitive chemical analysis by Raman spectroscopy. *Chemical reviews* **1999**, *99*, 2957–2975.

[91] Moskovits, M. Surface-enhanced spectroscopy. *Reviews of Modern Physics* **1985**, *57*, 783.

[92] Griffiths, P. R.; de Haseth, J. A. *Fourier Transform Infrared Spectrometry*; Wiley, 2007.

[93] Bellamy, L. J. *The Infrared Spectra of Complex Molecules*; CRC Press, 2004.

[94] Socrates, G. *Infrared and Raman Characteristic Group Frequencies: Tables and Charts*; Wiley, 2001.

[95] Koenig, J. L. *Infrared and Raman Spectra of Inorganic and Coordination Compounds*; Wiley, 1970.

[96] Lakowicz, J. R. *Principles of Fluorescence Spectroscopy*; Springer, 2006.

[97] Paddock, S. W. Fluorescence microscopy. *Advances in Biochemical Engineering/Biotechnology* **2000**, *66*, 107–135.

[98] Diaspro, A., Ed. *Confocal and Two-Photon Microscopy: Foundations, Applications, and Advances*; Wiley, 2010.

[99] Enderlein, J., Ed. *Single Molecule Spectroscopy in Chemistry, Physics and Biology: Nobel Symposium*; Springer, 2013.

[100] Alves, M. R.; Moreira, R.; Boaventura, R. A.; Santos, S. C. Surface modification of diatomaceous earth with ethylenediamine: application for atrazine removal from water. *Journal of Environmental Chemical Engineering* **2019**, *7*, 103236.

[101] Briceño, S.; Chavez-Chico, E. A.; González, G. Diatoms decorated with gold nanoparticles by In-situ and Ex-situ methods for in vitro gentamicin release. *Materials Science and Engineering: C* **2021**, *123*, 112018.

[102] Singh, J.; Bajaj, R.; Harpreet, K.; Harjot, K.; Navneet, K.; Sukhmeen, K.; Muhit, R. Chemo-bio synthesis of silver nanoparticles. *J Nanomed Res* **2016**, *4*, 00092.

[103] Mulfinger, L.; Solomon, S. D.; Bahadory, M.; Jeyarajasingam, A. V.; Rutkowsky, S. A.; Boritz, C. Synthesis and study of silver nanoparticles. *Journal of chemical education* **2007**, *84*, 322.

[104] Kurrey, R.; Deb, M. K.; Shrivas, K.; Khalkho, B. R.; Nirmalkar, J.; Sinha, D.; Jha, S. Citrate-capped gold nanoparticles as a sensing probe for determination of cetyltrimethylammonium surfactant using FTIR spectroscopy and colorimetry. *Analytical and bioanalytical chemistry* **2019**, *411*, 6943–6957.

[105] Mohd, N.; Zain, N. N. M.; Raoov, M.; Mohamad, S. Determination of carcinogenic herbicides in milk samples using green non-ionic silicone surfactant of cloud point extraction and spectrophotometry. *Royal Society open science* **2018**, *5*, 171500.

[106] Zamora Villón, J. V. Microfossils biostratigraphy and paleoenvironmental reconstruction of the late pleistocene lacustrine San Miguel formation, Guayllabamba basin, Ecuador. B.S. thesis, Universidad de Investigación de Tecnología Experimetal Yachay, 2020.

[107] Tesson, B.; Genet, M. J.; Fernandez, V.; Degand, S.; Rouxhet, P. G.; Martin-Jézéquel, V. Surface chemical composition of diatoms. *ChemBioChem* **2009**, *10*, 2011–2024.

[108] Gültürk, E.; Güden, M. Thermal and acid treatment of diatom frustules. *Journal of Achievements in Materials and Manufacturing Engineering* **2011**,

[109] Kim, Y.; Shinde, V. V.; Jeong, D.; Choi, Y.; Jung, S. Solubility enhancement of atrazine by complexation with cyclosophoraose isolated from Rhizobium leguminosarum biovar trifolii TA-1. *Polymers* **2019**, *11*, 474.

[110] Mercantili, L.; Davis, F.; Higson, S. P. Ultrasonic initiation of the alkaline hydrolysis of triglycerides (saponification) without phase catalysis. *Journal of Surfactants and Detergents* **2014**, *17*, 133–141.

[111] Plowman, B. J.; Tschulik, K.; Young, N. P.; Compton, R. G. Capping agent promoted oxidation of gold nanoparticles: cetyl trimethylammonium bromide. *Physical Chemistry Chemical Physics* **2015**, *17*, 26054–26058.

[112] Segneanu, A.-E.; Vlase, G.; Lukinich-Gruia, A. T.; Herea, D.-D.; Grozescu, I. Untargeted Metabolomic Approach of Curcuma longa to Neurodegenerative Phytocarrier System Based on Silver Nanoparticles. *Antioxidants* **2022**, *11*, 2261.

[113] Pal, J.; Deb, M. K.; Sircar, J. K.; Agnihotri, P. K. Microwave green synthesis of biopolymer-stabilized silver nanoparticles and their adsorption behavior for atrazine. *Applied Water Science* **2015**, *5*, 181–190.

[114] Song, X.; Li, H.; Al-Qadiri, H. M.; Lin, M. Detection of herbicides in drinking water by surface-enhanced Raman spectroscopy coupled with gold nanostructures. *Journal of Food Measurement and Characterization* **2013**, *7*, 107–113.

[115] Costa, J. C.; Ando, R. A.; Camargo, P. H.; Corio, P. Understanding the effect of adsorption geometry over substrate selectivity in the surface-enhanced Raman scattering spectra of simazine and atrazine. *The Journal of Physical Chemistry C* **2011**, *115*, 4184–4190.

[116] Meksiarun, P.; Spegazzini, N.; Matsui, H.; Nakajima, K.; Matsuda, Y.; Sato, H. In vivo study of lipid accumulation in the microalgae marine diatom Thalassiosira pseudonana using Raman spectroscopy. *Applied spectroscopy* **2015**, *69*, 45–51.

[117] Gannavarapu, K. P.; Ganesh, V.; Thakkar, M.; Mitra, S.; Dandamudi, R. B. Nanostructured Diatom-ZrO2 composite as a selective and highly sensitive enzyme free electrochemical sensor for detection of methyl parathion. *Sensors and Actuators B: Chemical* **2019**, *288*, 611–617.

[118] Rea, I.; De Stefano, L. Recent advances on diatom-based biosensors. *Sensors* **2019**, *19*, 5208.

[119] León Valencia, A. J. The optical properties of diatoms doped with plasmonic nanoparticles for biomedical applications. B.S. thesis, Universidad de Investigación de Tecnología Experimental Yachay, 2021.

[120] Agdi, K.; Bouaid, A.; Esteban, A. M.; Hernando, P. F.; Azmani, A.; Camara, C. Removal of atrazine and four organophosphorus pesticides from environmental waters by diatomaceous earth–remediation method. *Journal of environmental monitoring* **2000**, *2*, 420–423.